2019

Cosmic ray sensors for the continuous measurement of Arctic snow accumulation and melt

Anton Jitnikovitch
jitn4410@mylaurier.ca

Cosmic ray sensors for the continuous measurement of Arctic snow accumulation and melt

By

Anton Jitnikovitch

BSc, McMaster University, 2016

THESIS

Submitted to the Department of Geography and Environmental Studies in partial fulfillment of the requirements for

Master of Science in Geography

Wilfrid Laurier University

ABSTRACT

In the Arctic, winter persists for much of the year, resulting in a hydrological system that is primarily regulated by snow and snowmelt runoff, and has important implications on vegetation, animals, and on the thermal regime of the active layer and permafrost. Snow water equivalent (SWE) measurements such as remote sensing techniques provide coarse resolution data, while snow surveys and snow-pits are labour intensive, have limited spatial coverage and do not provide a continuous reading. Over the last few decades, cosmic ray sensors (CRS) have been proposed as a way to provide much improved snow data, but few studies have tested and used ground-based CRSs, and seldom in the Arctic. In this study we have used a ground-based CRS developed by Hydroinnova. This ground-based CRS can be installed in remote locations, deliver a continuous reading which can be monitored in real-time, and provide a point measurement with no practical limit to maximum SWE. In addition, individual ground-based CRSs can be installed along a transect to provide spatial details on snow accumulation and melt. The ground-based CRS was assessed at a high depth, high-SWE shrub patch environment in the western Canadian Arctic from October 2016 to June 2018 and a low depth, low-SWE rural landscape in Elora, Ontario from February 2017 to March 2018. Results indicate that the ground-based CRS at the high-SWE shrub patch and low-SWE rural site display Pearson correlation coefficients ranging between -0.89 to -0.98 and R^2 values ranging from 0.79 to 0.96 when comparing the moderated neutron intensity to manual SWE measurements from snow surveys. This research has the potential to enrich nivologic measurements and snow modeling by providing a continuous time series possessing information on the dynamics of ongoing meteorological events (snow accumulation, snowmelt and the impact of vegetation). Ground-based CRS sensors have the potential to provide SWE measurements for operational use such as

hydrological forecasting, water resource management, and flood and forest fire risk assessment. Over the long term, such measurements can also provide important data for assessing changes related to climate change.

ACKNOWLEDGEMENTS

I would like to thank my supervisor, Dr. Philip Marsh, for his mentorship, expertise, for the many thought-provoking conversations we have shared, and for sending me on multiple expeditions to the Canadian Arctic. Thanks to Matthew Tsui, Barun Majumder and Brampton Dakin for assisting in the collection of field data. Thank you to the entire Snow Hydrology lab group for their assistance in various parts of this dissertation. Special thanks to Dr. Aaron Berg for granting permission for the usage of the Elora Research Station site. Lastly, thank you to the Geography and Environmental Studies department as a whole for their inclusivity and benevolence; you are the reason Laurier is an exceptional university.

DECLARATION OF CO-AUTHORSHIP

I declare that I am the principal author of this thesis and all research within is the result of my personal production. This dissertation is the result of cooperation and collaboration with the co-authors listed in Chapter 2. Dr. Philip Marsh is the principal co-author whom has provided edits, revised the manuscript critically for important intellectual content, assisted with the conception and design of this study as well as the interpretation of data. Branden Walker is a co-author whom has provided background knowledge and assisted with the design of this study. Darin Desilets is a co-author and has provided background knowledge, literature sources, troubleshooting of the sensor instruments and in-depth expertise related to the interpretation of data.

Chapter 2 contains material that will be submitted to Arctic Science, a peer-reviewed journal.

DISCLAIMER

Any and all references made within this thesis to specific commercial products, services, manufacturers, trademarks, or otherwise, does not imply its recommendation or endorsement by Wilfrid Laurier University. All opinions and assessments of the author within this thesis do not reflect or represent Wilfrid Laurier University, and shall not be used for product promotion, endorsement, or advertisement.

TABLE OF CONTENTS

LIST OF TABLES

LIST OF FIGURES

LIST OF ABBREVIATIONS & EXPLANATIONS

SWE	Snow water equivalent
CRS	Cosmic ray sensor. Two types of CRSs exist, 1) ground-based sensors, which are installed on the ground surface and primarily measure downward directed cosmic rays (e.g. Hydroinnova's SnowFox), and 2) above-ground CRSs, which are installed above the ground-surface and mainly measure cosmic rays emitted from the soil (e.g. Hydroinnova CRS-1000/B).
SF	SnowFox
d_s	Depth of snow
p_w	Density of water
p_s	Density of snow
MSC	Meteorological Service of Canada
A	Albedo
COSMOS	COsmic-ray Soil Moisture Observing System
MCNPX	Monte-Carlo N-Particle eXtended
TVC	Trail Valley Creek
cph	Counts per hour. Referring to moderated neutron counts per hour
EDF	Électricité de France, a French electric utility company largely owned by the French state.
Hydroinnova	Company that designs, manufactures and markets specialized instruments for environmental observations. This includes cosmic ray sensors such as the SnowFox (SF) and 1000/B.
Pearson correlation (*r*)	A Pearson correlation is a measure of the strength of a linear association between two variables. Correlation coefficients (*r*) range from 0 (no relationship) to 1 (perfect linear relation) or -1 (perfect negative linear relationship). Negative correlation coefficients indicate an indirect relationship, meaning that when one variable increases, the other variable decreases. 0.10 to 0.29 represents a weak association between the two variables, 0.30 to

	0.49 represents a moderate association, and 0.50 and greater represents a strong association (Stats, 2013).
Simple linear regression	A simple linear regression is when an independent variable is used to predict the value of a dependent variable. Linear regression equation is output in a [y = m(x) + b] format (Stats, 2013). All regressions conducted in this work were set to a confidence interval of 95%.
R^2	The coefficient of determination (R^2) is the proportion of the variance in the dependent variable that is predictable from the independent variable. It is a measure of how well the regression line represents the data (Stats, 2013).

1. INTRODUCTION AND BACKGROUND

1.1 General Introduction

The Arctic is among the most rapidly warming regions on Earth (ACIA, 2005; Qu and Hall, 2006; IPCC, 2013; Tollefson, 2017). This warming has, and will continue to have a prominent impact on the Arctic and subarctic hydrological cycle. In particular, the duration of the Arctic winter season and snow cover has decreased considerably since the 1970s (Rees et al., 2014; Hori et al., 2017) but unfortunately, other vital aspects of the snow environment have not been explored sufficiently. This includes changes in snowfall, the impact of blowing snow on snow density, the effects of mid-winter thaw events, as well as the spatial variability in snow depth, snow water equivalent (SWE) and the rate and timing of spring melt. The inadequate assessments of these issues is largely due to the low density of manned observation stations across the extensive Arctic, significant errors related to ground-based snow survey measurement methods, and a lack of suitable remote sensing methods.

Seasonal snow covers 46 million square kilometers of Earth's surface. This snow cover has been decreasing consistently since the 1970s (Derksen and Brown, 2012; NSIDC, 2017; Hori et al., 2017) and has led to the integration of complex predictive models to estimate how Earth's climate may transform. Current projections indicate that due to climate warming, the northern hemisphere snow season will continue to shorten, ultimately leading to a 10-20% decrease in snow cover by 2100 (NRC, 2011; IPCC, 2013). Although there are on-going improvements towards introducing additional snow observations stations in the Arctic (Schiermeier, 2006; Goodsite et al., 2016; CNNRO, 2016), the complications related to obtaining continuous snow measurements in remote regions have not been properly addressed. Prominent instrumental options to record SWE include ultrasonic, ground and airborne LIDAR, and gamma-based

systems. Unfortunately, ultrasonic systems have inherent measurement issues related to changes in temperature, the presence of strong winds, and when measuring soft or irregular surfaces (Kinar and Pomeroy, 2007). LIDAR systems have difficulties measuring complex terrains and forested sites (Deems et al., 2013), while gamma-based sensors have limited ability to measure deep snowpacks (Paquet et al., 2008) which are commonly found in the Arctic (Marsh and Woo, 1981; Gray et al., 1989).

By having continuous snow data throughout a winter season, the total meltwater, as well as the timing and magnitude of runoff, can be determined (Harshburger et al., 2005). Since changes in the snowpack have important consequences for Earth's environment and its inhabitants, such as impacts on the regional and global climate (Rees et al., 2014), ecology, and water resources, it is essential that new techniques for continuous snow measurements are developed. Cosmic ray sensors (CRS) (Desilets et al., 2010; Zreda et al., 2012; Sigouin and Si, 2016; Schattan et al., 2017) have been suggested as a possible approach to provide continuous snow data and can measure SWE at a point or over a domain of up to 18 ha (Köhli et al., 2015), depending on the type of sensor. Kodama et al. (1979) first utilized cosmic rays to measure SWE by burying a shielded neutron sensor below the ground surface and allowing snow to accumulate upon it. It was noted that the CRS recorded neutrons in the fast to epithermal range, which are carried by Earth’s magnetic field and weakened by colliding with hydrogen atoms in the snow until some neutrons reach a suitable energy level to penetrate the CRS instrument casing (shield). Kodama et al. (1979) determined that a strong negative correlation exists between the neutron count and SWE due to the neutron moderating characteristics of hydrogen.

Recently, a number of networks of cosmic ray sensing instruments for soil moisture and snow applications have been installed and continue to expand (Paquet et al., 2008; Zreda et al.,

2012; Delunel et al., 2014). These networks are used for hydrometeorological and agricultural applications, to estimate the contribution of winter snowmelt to hydroelectric power plants, and to assist in surface- and groundwater modeling. Ultimately, these CRS networks indicate the potential for using cosmic rays to provide continuous measurements in remote locations, and in troublesome terrains such as vegetation patches, ridges and mountain overhangs. Over the short term, data obtained from CRSs may provide key inputs for water resource management, while over the long term, it may provide insight to understanding how the climate and hydrology is changing.

1.2 Thesis Objectives and Overview

Following this overview, Chapter 1 consists of background information discussing the importance of snow physical properties and various measurement methods. This chapter also discusses the history, theory and current applications of cosmic ray sensors. Chapter 2 is written in manuscript format and will be submitted to Arctic, a peer-reviewed journal. The manuscript examines the application of cosmic ray sensors for the measurement of snow water equivalent (SWE) with a focus on its practicality in the Arctic. This was achieved by:

1) Determining the accuracy of the ground-based CRS at a point scale in both shallow (low-SWE) and deep (high-SWE) snowpacks, and
2) Assessing the variability of snow accumulation and melt of a large snowdrift over two winter seasons using multiple ground-based CRSs strung together in a transect.

The accuracy of the ground-based CRS was determined by comparing manual measurements from snow surveys to SWE values obtained from the CRS. The Summary and Conclusions section (Chapter 3) summarizes the findings from Chapter 2 and discusses areas of interests for

future research surrounding cosmic ray sensors. Tables and figures containing background information have been included in the appendix. The final section contains the references used in this research. It is important to note that because of the manuscript format, this thesis contains some repetitiveness.

1.3 Snow Data Applications

Snow data is used for multiple applications and by various groups and organizations ranging from researchers, small- and large-scale businesses, and all levels of government. These groups implement snow data into complex models (Nester et al., 2012; Abudu et al., 2012; NWS, 2017) in order to predict stream flow, and to aid in flood forecasting, water resource management, wildlife management (such as migration timing and routing), and structural design of buildings and bridges. A rapid snowmelt may lead to flooding or an excessively large stream flow, which can cause infrastructure damage and road closures (Buska and Tobiasson, 2001), as well as impact logistics and other activities, such as hunting or fishing (Niehaus and Ydenberg, 2006; Liebezeit et al., 2014; Seebacher and Post, 2015; Nicholson et al., 2016). Additionally, predicting snow melt runoff and stream flows is crucial for the management of hydroelectric dams and water resources in general (Turcotte et al., 2004; NTPC, 2013). Considering wildlife migration timing and routes are impacted by seasonal cues (Niehaus and Ydenberg, 2006; Seebacher and Post, 2015) rapid melt may lead to flooding and ultimately alter animal migration patterns. It is also important to note that snow depth, density, and SWE data are used to establish snow load guidelines in order to maintain the structural integrity of buildings (Buska and Tobiasson, 2001; FEMA, 2013).

1.4 Snow Measurement Variables

The physical properties of snow that are of most interest to hydrologists include the snow depth (d_s), density (p_s), and water equivalent (SWE). Other properties of snow such as grain size, strength, etc., are also of interest, but will not be considered here. Snow depth is defined as the vertical distance from the snow surface to the ground and is commonly obtained by using a portable measurement rod during snow surveys or by ultrasonic or laser sensors installed on automated weather stations (Mair and Baumgartner, 2010). At larger scales, snow depth is often measured using gamma radiation, ground and airborne LIDAR, visible/near infrared, and passive microwave remote sensing techniques (Engman and Gurney, 1991; Dietz et al., 2012).

The density of snow is defined as the snow mass in a known volume. The mass of a snow sample is often determined by weighing it immediately after obtaining the original snow/snow-core. A known (or reference) volume is obtained by a snow "density-cutter" of a predetermined volume. Alternatively, if using a snow tube, the user will note its volume beforehand. Since snow typically varies considerably over short distances and due to factors such as recrystallization, compaction, sublimation and blowing snow, this method should be conducted multiple times to maximize accuracy (Pomeroy and Gray, 1995). When the mass and volume are known, the density is calculated (equation 1.1).

$$\text{Density} = \text{Mass}_{(\text{Snow})}/\text{Volume}_{(\text{Container})} \quad \textbf{(1.1)}$$

Snow water equivalent (SWE) is the amount of water contained within a snowpack and is defined as the depth of water when the entire snowpack has melted.

SWE is generally calculated based on the density of water (p_w):

$$SWE = d_s \times (p_s/p_w) \quad \textbf{(1.2)}$$

Where SWE is in m, d_s is in m and p_s and p_w are in kg/m^3. It is common practise when calculating SWE to assume the density of water to be 1000 kg/m^3, therefore the equation is commonly abbreviated to:

$$SWE = Depth \times Density \quad \textbf{(1.3)}$$

Common approaches to measuring SWE at small-scales include snow pillows, snow tubes, and snowpits.

1.5 Manual Snow Depth Measurements

Field measurements of snow depth are commonly obtained using a portable measurement rod. The rod is inserted vertically through the snow surface until it reaches the snow/soil interface, at which point, the user records the depth. Snow depth recordings are used for structural, civil and environmental engineering purposes (Goodison et al., 1981), to understand the geographic distribution of wildlife (Schwab and Pitt, 1991), and paired with density measurements to determine SWE which can be input into hydrological models (DeBeer and Pomeroy, 2010). The measurement rod is commonly a metal stick with rigid markings on its surface indicating the measurement value. When measuring deeper snowdrifts (greater than 2 m) an ‘avalanche stick’ is used. This is a portable measurement rod with metallic screw threads on both ends which allow the rod to be coupled together (multiple attachments if necessary). Snow depth measurements are usually acquired in transects which can range to 100's of meters in size.

Snow transects can range in size from containing single-digit to dozens of depth measurement points and density measurement samples. Due to large transect sizes and the time consumption involved with snow depth measurements, Sturm (1999) designed a self-recording snow depth device called a GPS Snow Depth Probe or MagnaProbe. The MagnaProbe uses a sliding disc attached to an electromechanical rod that when inserted vertically into the snowpack, the length between the ground/soil and snow/atmospheric interface is delineated. As the MagnaProbe reaches the ground surface, the user presses a trigger and the internal data logger records the distance between the bottom tip of the rod and the sliding disc sitting on the snow surface. Immediately after the depth is recorded by the MagnaProbe, the GPS coordinates are recorded as well. The GPS on a typical Magnaprobe is a Garmin product, which provides an accuracy of +/- 10 m (please note that most of this error is in the elevation). Using this probe, the user can walk across a snow-blanketed landscape and produce a detailed transect of snow depths. The Magnaprobe data logger can store thousands of depths and is easily transferable via memory stick.

1.6 Manual Snow Density Measurements

Church (1933) introduced the use of snow tubes as a standard in the manual measurement of snow through snow surveys. Snow tubes are commonly made of metal or transparent plastic with a notched cutting end (Crook and Freeman, 1973). The transparent plastic tubes have the advantage that the user can clearly see the snow sample after it has been extracted. The metal snow tubes possess a vertical opening running down the side allowing for visual clarification. The snow tube samples are obtained by vertically inserting the tube into the snow surface until it has reached the soil/snow interface. At this point, the user pushes down on two handles attached to the snow tube and turns until the notched end acquires a plug of soil at the base, trapping the

overlying snow sample. The user then carefully transfers the snow into a Ziploc bag and removes the soil plug. The snow-filled Ziploc bag is then weighed using a calibrated spring or electronic scale. The mass and density are then recorded and used for SWE calculations. Snow tube sampling alters the snowpack during each sample and is therefore an invasive technique (Smith et al., 1967).

Common snow tubes used in Canada are the Standard Federal, the Meteorological Service of Canada (MSC), and the SnowHydro (Dixon and Boon, 2012). The oldest is the Standard Federal, developed and used in the early 1930s (Church, 1933; Goodison et al., 1981). It is an aluminum tube possessing an orifice of small diameter (60 mm), with notched ends that are used for attachment pieces. The Standard Federal is designed for deep alpine snowpacks, and therefore has the capability to take a snow-core sample up to 5 meters in depth. This snow tube has its own unique calibrated spring-scale which allows for the measurement of SWE on-site (Clyde, 1932). It is important to mention that wind-conditions can lead to discrepancies when using the spring-scale. Thus, an alternative is to collect samples and weigh them in a controlled laboratory setting afterwards or to use a calibrated electronic scale.

The MSC and SnowHydro are larger diameter tubes which increase the accuracy of measurement and are well-suited for shallower snow. The MSC can obtain snow samples up to a depth of 1 m while the SnowHydro up to a depth of 1.6 m (Goodison, 1978; Goodison et al., 1981; SnowHydro, 2004). In contrast to the Standard Federal snow tube, the SnowHydro is only available in a transparent Lexan material while the MSC in both aluminum and Lexan. The MSC snow tube has 16 cutter teeth and is similar in design to the Standard Federal 16 cutter teeth model. In contrast, the SnowHydro possesses only 12 teeth and due to its transparent design,

does not require any observation slots such as those in the Standard Federal or some models of the MSC snow tube (Goodison et al., 1981; SnowHydro, 2004).

Multiple studies have analysed the issues associated with snow tube sampling (Bindon, 1964; Freeman 1965; Work et al., 1965; Beaumont, 1967; Peterson and Brown, 1975; Goodison, 1978; Farnes et al., 1982, Sturm et al., 2010). Each study found that the Standard Federal and the MSC snow tube tended to overestimate SWE when compared to measurements from adjacent snow pits. From these analyses it was determined that the Standard Federal overestimates anywhere from 1% (Sturm et al. 2010) to 11.2% (Beaumont, 1967), with an average overestimation value of 8.3%. Furthermore, Goodison (1978) and Farnes et al. (1982) conducted an in-depth analysis of the MSC snow tube by comparing SWE values to adjacent snow pits and determined that the MSC snow tube overestimates by 6-7%. Contrarily, the SnowHydro is the only snow tube that tends to both over- and underestimate SWE values, with a discrepancy range of -9 to 10% (Sturm et al., 2010). Some of the common reasons for measurement error associated with snow tubes includes the design of the cutting teeth, the presence of vertical slots along the snow tube and human error (Goodison et al., 1981). For the field work component of this thesis, the SnowHydro snow tube was used. This snow tube was chosen because it has been proven to work in harsh Arctic conditions (SnowHydro, 2004; Dixon and Boon, 2012).

1.7 Other Snow Measurement Techniques

1.7.1 Snow Pits

Several other common snow measurement techniques exist, each with their own unique set of strengths and weaknesses. One of these techniques is the use of snow pits. A snow pit is a large burrow dug in the snow (down to the ground surface) using a shovel. The ground surface serves as the reference datum. It is generally created when the user wishes to delineate different

snow events and assess in-detail the snow stratigraphy by taking note of the varying densities throughout the snowpack. The snow pit technique allows the researchers to better understand snowpack metamorphism, which has potential to enhance snow modeling, and improve avalanche predictions (Williams et al., 2010). However, some issues associated with snow pits include the laborious task of creating them, the invasiveness of the technique, and the lack of continuous readings (Kinar and Pomeroy, 2015). These factors represent considerable limitations when working with remote, high depth snowpacks where several measurements are required over an extended period of time, and digging multiple snowpits several meters in depth is not practical.

1.7.2 Snow Pillows

Snow pillows are a common pressure sensor which continuously record point measurements of SWE at an established location (Kinar and Pomeroy, 2015). They are generally a rectangular or circular pressure transducer buried in the ground surface, allowing snow to fall upon it (Molnau, 1971; Johnson, 2004). The pressure sensor is filled with an anti-freeze chemical allowing a pressure gauge device to sense the overlying mass of snow by noting the changes in fluid pressure (Beaumont, 1965). This change in fluid pressure is then converted to SWE. Snow pillows are essentially a permanent structure, therefore the task of building them on-site could be challenging and expensive. Since snow pillows are often set-up in remote locations, logistical factors must be considered. In addition, because the pressure transducer is filled with anti-freeze liquid, this can lead to multiple complications occurring in oftentimes pristine environments, such as a mechanical abrasion that has potential to cause leakage (Ord, 1968). It is also important to note that wildlife could damage or impact the results of the snow pillow (Shannon, 1968; Davis, 1973). Measurement error could arise from snow pillows because of the shear stress exerted due to the variance in compressibility between the surrounding snow and the pillow

itself. Additionally, the difference between the physical and thermal properties of the snow pillow and the surrounding snowpack, can lead to a discrepancy in melting rates (Johnson, 2004; Johnson and Marks, 2004; Kinar and Pomeroy, 2015). Lastly, snow pillows commonly have errors due to the formation of ice layers and when a shallow snow cover is present (Krajči et al., 2017).

1.7.3 Remote Sensing Techniques

Remote sensing is a prominent approach in snow hydrology that is used to quantify aspects of the snow cover without making physical contact with the snow itself (Seidel and Matinec, 2004; Pullianen, 2006; Takala et al., 2011; Deems et al., 2013; Painter et al., 2016). Although remote sensing includes large scale data monitoring, data acquisition at multiple resolutions, and a reduction of field work, there are several inherent disadvantages from using these techniques as well. The most prominent remote sensing approaches will be briefly discussed in this section.

1.7.3.1 Gamma Radiation

Gamma-based remote sensing takes advantage of the low-level radiation that minerals found in soils naturally emit (such as potassium and thallium). Gamma detectors may either be ground-based, or airborne. Airborne gamma sensors mounted on aircraft make flights over a designated route before any snow cover and then again after a snow cover is present. This allows the aircraft to record the change in attenuation between the snow-free and snow-packed site (Carroll and Vadnais, 1980; Seidel and Matinec, 2004). Since a higher water content will cause a higher attenuation of the gamma rays, a SWE value can be inferred. Unfortunately, due to the principle of gamma-based systems, they are limited to relatively flat terrains. This is because the atmosphere naturally attenuates a significant portion of the radiant energy, therefore aircraft must

fly at low altitudes (approximately 150 m) in order to capture the gamma signal. Additionally, gamma-based remote sensing is inherently limited to a shallow SWE measurement depth (Vershinina, 1985), and has difficulty measuring in forested areas due to the effect of forest biomass weakening the radiation signal (Glynn et al., 1988).

1.7.3.2 LIDAR

Like gamma-based remote sensing, LIDAR (light detection and ranging) systems can be airborne or ground-based. LIDAR systems send a laser pulse which measures the target distance based on the elapsed time between the transmitted and returned signals of energy. This approach works by taking datasets from at least two different dates and differencing them (Deems et al., 2013). One of these dates must include a snow-free site, and the other snow-covered. The most prominent use of LIDAR for snow measurements is conducted by NASA's Airborne Snow Observatory (Painter et al., 2016). Unfortunately, this approach is only able to measure snow depth and therefore must be combined with other approaches in order to measure SWE. Additionally, LIDAR has the potential for high operating costs (Deems et al., 2013), measurement issues related to dense canopies, and can be unreliable during wet weather conditions (Engman and Gurney, 1991) which are becoming more frequent in a warming Arctic (Tollefson, 2017).

1.7.3.3 Visible/Near Infrared

The visible and near-infrared section of the electromagnetic spectrum contains a wavelength between 400 and 1400 nanometers (nm) (Moseley and Zabierek, 2006). This wavelength is a combination of the entire visible spectrum with the neighbouring section of the infrared spectrum up to the water absorption band (Waiser et al., 2007). Snow cover can easily be classified and mapped using a wavelength between 400 and 700 nm because of the high

reflectance value in contrast with no-snow areas. Snow reflectance is often termed as the albedo of the snow surface. The albedo (*A*), is defined as:

$$A = \text{Reflected solar radiation/Incoming solar radiation} \quad \textbf{(1.4)}$$

Since this remote sensing technique corresponds to the visible channels, aircraft or unmanned aerial vehicles can be equipped with a visible/near infrared sensor to measure snow properties. Alternatively, if using satellite imagery, the user will select the NOAA VHRR channel, the Landsat MSS channels 4 and/or 5, SPOT, or the Landsat TM channels 2 and/or 4 to assess snow properties (Dozier, 1984). Choosing the appropriate spectral band is crucial since a less appropriate selection may lead to a loss of detail in delineating snow and no-snow areas. Although snow reflectance can be detected in the near-infrared region, the disparity between a snow covered and no-snow covered landscape is noticeably decreased. Therefore, not only is it vital for the user to select the appropriate band for an accurate analysis, but also for the user to be trained in delineating snow and no-snow landscapes using these spectral bands.

1.7.3.4 Passive Microwave

Passive microwave remote sensing is the most common remote sensing technique used by snow hydrologists. This approach provides multiple advantages over other remote sensing techniques such as information on the snow cover extent, snow depth, SWE, as well as the ability to detect the onset of melt (Kunzi et al., 1982; Pullianen, 2006; Takala et al., 2011). The snowpack characteristics are responsible for its microwave properties. Microwave radiation that is emitted from the ground surface underlying the snow is scattered in various directions due to the snow grains in the snowpack, leading to a microwave emission at the top of the snowpack

being less than the ground emission. Since the amount of scattering in a snowpack is proportional to the depth and density, SWE can be related to the luminosity temperature of the specific site (Hallikainen and Jolma, 1986; Pullianen, 2006); shallow snowpacks will result in a higher luminosity temperature and vice versa. Unfortunately, most passive microwave sensors have a spatial resolution of 25 km and are not well suited to track or model small or landscape-scale changes of snow properties (Thirel et al., 2013). Additionally, microwave remote sensing SWE readings saturate at values greater than 12 cm (Derksen, 2008). The Globsnow SWE report is a prominent example of an approach utilizing passive microwave data combined with ground-based weather station data to create a long-term SWE record. A more in-detailed explanation of the theory behind microwave radiation remote sensing for SWE is given by Pomeroy and Gray (1995) and Pulliainen (2006).

1.8 Cosmic Ray Sensor

In 1912, the physicist Victor Francis Hess, made multiple flights using a hot-air balloon in order to take radiation measurements at altitudes reaching up to 5.3 km (Joseph, 2004). Hess noted that the level of radiation recorded was standard until reaching an altitude of 1 km. Past this height, radiation levels began increasing, and at 5 kilometers Hess found them to be approximately two times more potent than at 1 kilometer. This led Hess to conclude that radiation was driven from outer space. Robert Millikan would later confirm this discovery and termed this outside radiation as ‘cosmic-rays’. In 1935, another advancement to the topic came when Arthur Compton noted that the cosmic rays discovered by Hess and confirmed by Millikan, were linked to secondary radiation in the cosmic-ray flux, while primary radiation was composed of electrically charged particles which initially entered Earth’s upper atmosphere and led to the formation of these secondary cosmic rays. Decades later, researchers from Japan

attempted to use these secondary cosmic-rays for snowpack applications in 1979 and soil moisture applications in 1985.

1.8.1 Secondary Cosmic-Rays and their Significance to Polar Regions

All matter is made of subatomic particles such as electrons, protons, and neutrons. Hydrogen, the most common and lightest element, is made of an electron and a proton. Up to 90% of primary cosmic rays are made up of a hydrogen nuclei, 9% of a helium nuclei, and the rest are consisting of heavier elements (Zreda et al., 2012; Sigouin and Si, 2016). Primary cosmic rays possess extremely high energies (GeV range), travel at nearly the speed of light, and have a galactic or solar origin (Bartol, 1999; Zreda et al., 2008; Zreda et al., 2012). As these extremely high energy cosmic rays enter the Earth's atmosphere, they collide with atmospheric nuclei (usually nitrogen or oxygen) and cause a cascade of secondary cosmic rays which are 'carried' by Earth's magnetic field towards the Polar Regions. There are multiple types of secondary cosmic rays such as pions, electrons, muons, photons, x-rays, alpha particles, and neutrons. The secondary cosmic rays of interest in this thesis are neutrons. As these secondary cosmic rays continue colliding with atmospheric atoms, their energy levels decrease with each collision. Eventually, after traversing through the snowpack and being further attenuated by hydrogen, some of these secondary cosmic rays will reach the Earth's surface with an energy level of ~1 MeV or less (Zreda et al., 2012). At this energy level, a neutron is able to be absorbed by the CRS. An illustration of cosmic ray movement can be seen in the appendix (Fig. A.1).

Earth's magnetic field acts as a defensive shield against the majority of primary and secondary cosmic rays (Bartol, 1999). These rays begin to interact with the Earth's magnetic field about 60,000 km above the Earth's surface. At this altitude, the primary cosmic ray particles begin to experience Earth's magnetic field which 'carry' the particle towards the Polar

Regions. A primary cosmic ray collides with an atmospheric nuclei about 20 km above the Earth's surface, creating a shower of secondary cosmic rays, for example neutrons (Bartol, 1999). These collisions continue until the secondary cosmic ray energy level has been attenuated to an appropriate magnitude and is able to be detected by a CRS. It is important to note that only the highest energy cosmic rays are able to penetrate the magnetic field, and Earth's atmosphere, to reach the ground at the equator (Bartol, 1999). For this reason, it is crucial to measure cosmic rays in extreme latitudes such as the Polar Regions.

1.8.2 Hydrogen Attenuation

CRSs measures moderated neutrons in a 'neutron per unit time' framework, also known as the neutron intensity. This time interval is generally set to one hour. The moderation of fast neutrons, sometimes referred to as "slowing down", is the loss of energy that occurs due to a neutron colliding with nuclei. Moderation causes fast neutrons to eventually lead into slower (lower energy) neutrons. Hydrogen has the largest moderation ability compared to other elements due to its energy decrement per collision. The energy decrement per collision is inversely proportional to the atomic mass of the nucleus (Desilets et al., 2010; Zreda et al., 2012; Siguoin and Si, 2016). Hydrogen has a very small atomic mass and therefore neutrons require fewer collisions in order to convert a high energy neutron into a lower energy neutron. Due to the dominant 'slowing down' characteristic of hydrogen, it is a significant part of neutron recordings in the atmosphere, surface, and soil interfaces. With this approach the CRS-measurements do not discriminate against wet snow, ice lenses, or dry snow; a prominent advantage over conventional methods. During times of high barometric pressure, more hydrogen will be present in the atmosphere, which will increase the amount of collisions that neutrons undertake before reaching the CRS. It is important to note that some types of CRSs (eg. Hydroinnova's 1000/B model) are

able to record neutrons attenuated by elements other than hydrogen such as potassium, boron, and chlorine, however, this attenuation approach is used for soil moisture measurements and not snow.

1.8.3 Cosmic Ray Sensor Instrument Overview

1.8.3.1 Ground-based Cosmic Ray Sensor Overview

The instrument used in this research is a ground-based CRS developed by Hydroinnova and called the SnowFox. This CRS is a portable, affordable and highly adaptable sensor capable of providing point measurements (1 m^2) of SWE. The CRS is placed on the ground where it is allowed to be buried by falling snow (Fig. 1.1) and because of this, is considered a ground-based CRS. The sensor is programmed to record in a pre-set time interval (generally 1-h) the intensity of downward directed neutrons which traverse through the snowpack. This magnitude is directly related to the attenuation of neutrons through the overlying snow and is related to SWE by incorporating a correction function. As a result, the ground-based CRS provides a point measurement which has been shown to measure up to 57 cm of SWE (Howat et al., 2018) and has capabilities to measure at least 4 meters and potentially up to 10 meters of SWE (Howat et al., 2018).

There are two natural factors that affect the number of neutrons reaching the CRS. The first and more significant factor is the barometric pressure. As secondary cosmic rays collide with atmospheric particles, the successive collisions are inversely dictated by the number of particles found per unit volume of air. This means that with a higher atmospheric pressure (more atmospheric mass) the number of particles per unit volume of air increases, and the scattering mean free path for neutrons is decreased, allowing fast neutrons to (on average) travel a shorter distance before becoming slower neutrons. The opposite holds true as well, with increasing

elevation (decreasing air density) the scattering mean free path for neutrons increases, causing fast neutrons to travel a further distance before their energy is reduced.

The second, less influential factor is the incoming temporal cosmic ray flux, also known as the solar factor. Due to the natural variation of solar radiation, it is critical to correct the solar factor by incorporating counts from a neutron monitor into equation 2.3. The Inuvik Neutron Monitor data was used to correct the solar factor in this work. It is important to note that although the ground-based CRS detects downward directed cosmic-rays, some neutrons are detected by the CRS due to a backscattering effect that occurs when a neutron with a sufficient energy level penetrates the soil, scatters back, and collides with the CRS. Because of this, having reliable knowledge of the soil water storage before the initial winter freeze is vital for low-SWE environments if the ground-based CRS sensor was not set up before the freeze-up occurred (because the CRS baseline did not incorporate pre-winter conditions) (Paquet et al., 2008; Siguoin and Si, 2016). Knowledge of this antecedent water content is critical because the ground-based CRS measurement principle works via an attenuation by hydrogen. For the purposes of this work, the ground-based CRS's baseline is obtained by setting up the instrument 7-14 days prior to the initial snow-precipitation events of the season.

The ground-based CRS sensor is a 130 cm cylindrical detector tube with a control module incorporating a Hydroinnova QDL2100 data logger as well as an iridium satellite communication device. The detector tube contains ^{3}He gas, this gas is used due to its stability. The detector tube is considered moderated (shielded) due to its polyethylene and lead casing and measures high energy neutrons (~1 MeV or less) which traverse through the snowpack and are attenuated by hydrogen. It is important to note that prior to hydrogen attenuation these neutrons are considered to be of an extremely high energy (larger than 1 MeV). As these neutrons

attenuate to an energy level of ~1 MeV and collide with the ground-based instrument, they penetrate the polyethylene and lead casing causing the high energy of the neutron to be reduced to about 1/40th of an electron volt. At this point, a helium atom in the detector tube absorbs the neutron and splits into a lithium ion. This ion removes electrons from neutral atoms in the detector tube and produce a charge in the tube of gas. This newly charged ion is then detected and amplified by a built-in amplifier inside the CRS. The sensor then records this as 1 neutron count (Bartol, 1999). This process continues over the pre-set measurement interval (generally 1-h) and is automatically posted in real-time on a private web portal provided by Hydroinnova.

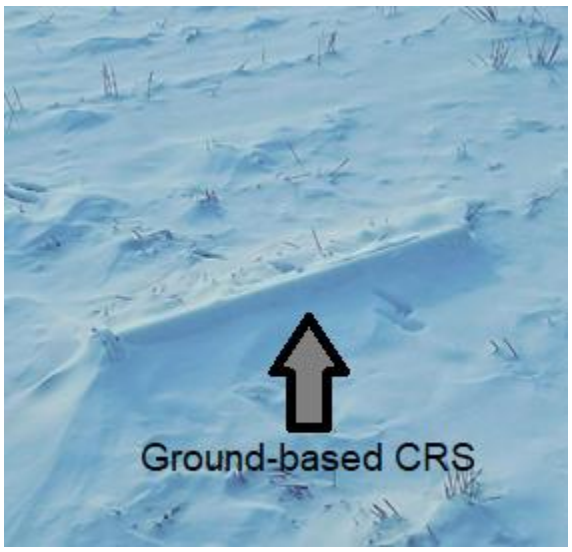

Figure 1.1. Partially snow-covered ground-based cosmic-ray sensor (CRS) installed at the Elora site in Ontario.

1.8.3.2 1000/B Cosmic Ray Sensor Overview

Another Hydroinnova CRS model is the 1000 and its variation, the 1000-B. The main differences between the CRS 1000 and 1000-B models is that the 1000 is smaller, lighter and has a smaller power consumption. Alternatively, the 1000-B costs less and has better humidity

protection. Both models operate using a similar principle as the ground-based CRS, however, unlike the ground-based CRS which has only one moderated detector tube, the 1000/B is an above-ground CRS characterised by two detector tubes (moderated and unmoderated) and a control module. Each detector tube measures neutrons of different energy levels. The moderated (shielded) tube measures high energy neutrons while the unmoderated (unshielded) tube records lower energy neutrons. The higher energy neutrons are faster moving and are attenuated by hydrogen while the lower energy neutrons are affected by hydrogen and other elements such as K, B and Cl in the soil, soil/snow interface and potentially some parts of the snowpack (Desilets et al., 2010; Zreda et al., 2012; Sigouin and Si, 2016). Due to the small atomic mass of hydrogen, the speed of penetration of neutrons throughout the snowpack is considered fast, as this atomic mass increases (due to different elements in the medium), the energy of neutrons is decreased and is measured by the unmoderated tube. Therefore, the moderated tube is used to measure SWE while the unmoderated tube is used to measure soil moisture. The primary advantage to using an above-ground CRS model is the ability to estimate SWE in a landscape-scale approach. Originally this scale was stated to be a 300 m radius at sea level (Desilets and Zreda, 2013), however, recent literature suggests this value is closer in range to 130-240 m and is dependent on environmental factors such as air humidity, soil moisture and vegetation (Köhli et al., 2015). More details on how cosmic ray sensors measure neutrons can be found in Desilets et al. (2010) and Zreda et al. (2012).

Although considered negligible in a ground-based CRS, research involving above-ground CRSs incorporate atmospheric water vapor into their correction equation (Desilets et al., 2010; Rasmussen et al., 2012; Sigouin and Si, 2016; Wrona, 2016; Schattan et al., 2017). This is because as the water vapor in the troposphere increases, neutrons travel a shorter distance before

colliding with another hydrogen atom, effectively shortening the scattering mean free path and causing the above-ground CRS to experience a decline in neutron intensity. Although the above-ground CRS is considered a more sophisticated sensor than the ground-based CRS – due to its capability in measuring SWE within in a landscape-scale footprint, an inherent disadvantage is that it is only able to provide an average SWE value over an area, has a maximum SWE saturation ranging from 5.8 cm to 70 cm (depending on soil moisture) (Zreda et al., 2008; Sigouin and Si, 2016), and is not able to analyse the accumulation or melt of large drifts, specific snow patches or be used to measure SWE along ridges and/or mountain overhangs (while the ground-based CRS can).

1.8.4 Current Applications and Potential Future Uses

Most current applications using a CRS are focused on an above-ground model, the 1000/B, which was originally developed for soil moisture measurements. The largest network of above-ground CRSs is the COsmic-ray Soil Moisture Observing System (COSMOS) which has over 48 sensors set up throughout the United States as well as several in Canada, Australia, Brazil, Europe, and Africa (Zreda et al., 2012). The COSMOS team has plans to expand this network to a total of 500 cosmic ray probes deployed internationally. In addition, Électricité de France (EDF), a French electric utility company largely owned by the French state, has set up a network of about 40 cosmic ray snow gauges throughout the French Alps, Pyrenees, and Massif Central to quantify the contribution of winter snowmelt towards their hydroelectric power plants (Paquet et al., 2008; Delunel et al., 2014). Although EDF uses a ground-based CRS, their design is different than the ground-based CRS version produced by Hydroinnova. EDF's CRS is designed with a box-shaped polyethylene shield of 12 cm thickness on the side and 7 cm on both the top and bottom of the detector, while the Hydroinnova instrument has a uniform cylindrical-

shaped polyethylene shield about 7 cm in thickness. This variability in thickness is meant to minimize the effects of soil-water content on fast neutron monitoring (Desilets et al., 2010; Delunel et al., 2014).

Using a homogenous landscape with low-lying vegetation, several studies have shown that the CRS 1000-B is able to measure soil moisture with considerably accuracy (Zreda et al., 2008; Desilets et al., 2010; Coopersmith et al., 2014). One study conducted in the Western Canadian Arctic by Wrona (2016) noted that the above-ground CRS was most sensitive to the moisture signal in the top 5 cm of soil and not the estimated effective sensing depth of 10 cm. Wrona notes that this discrepancy may be due to a missing hydrogen source (such as soil organic carbon) which was not accounted for. Ultimately, Wrona (2016) determined that the correction used to measure soil moisture was site-specific and not transferrable to other Arctic tundra locations. Another application to measure soil moisture using a modified above-ground CRS was conducted by Chrisman and Zreda (2013). This study attempted to innovate the intermediate-scale approach by placing a mobile and larger version of the CRS 1000-B in the back of a pickup truck and mapping soil moisture over large areas. Chrisman and Zreda (2013) mapped soil moisture 22 times in a 25 km by 40 km area, in Tucson Basin, Arizona, however, they noted large variations in soil water content measured by the CRS which may have been attributed to the extremely short pre-determined counting rate interval. Commonly this counting rate interval is set to 1-hour, however the mobile CRS had its neutron counting rate interval set between 1-7 minutes. Another study tested the effectiveness of detecting soil moisture using rover surveys with a focus on the influence of local structures and roads (Schrön et al., 2017). Using neutron transport simulations and dedicated experiments, it was found that depending on the road material, width, the surrounding field water content and distance from the road, the above-

ground CRS could overestimate soil moisture by up to 40% (Schrön et al., 2017). Further study on this topic should be explored.

Presently, the rising topic concerning ground-based and above-ground cosmic ray sensors revolves around the measurement of SWE. Desilets et al. (2010) noted that these sensors could be used for measuring SWE since snowfall causes rapid drops in the neutron intensity. Desilets et al. (2010) found that the calculated SWE values from the CRS corresponded closely to manually obtained data from snow surveys. CRSs ability to measure SWE was expanded when Sigouin and Si (2016) set up an above-ground sensor at an agricultural field in Saskatoon, Saskatchewan and were able quantify SWE up to 7 cm. They determined an empirical formula to estimate SWE at their site by conducting a linear regression which yielded an R^2 value of 0.81. The following season they noted that the CRS-estimated SWE compared well to snow surveys and snow depth correlations from nearby sites. Another recent study using CRSs was conducted by Schattan et al. (2017), who tested an above-ground sensor in an alpine snowpack in the Austrian Alps. From March 2014 through June 2016, this group collected neutron data from the sensor, conducted manual snow survey measurements and then compared the results using a terrestrial laser scanner at the same site. Their results noted that the above-ground CRS can accurately record up to 60 cm of SWE in a ~240 m footprint – almost 6 times more than the amount recorded in prior works (previous studies measuring SWE with the 1000/B have been limited to 7-12 cm of SWE). The most recent CRS study was conducted by Howat et al. (2018) who installed a ground-based CRS on a glacier in Greenland in April 2016. After correcting for variability in atmospheric pressure and the incoming cosmic radiation, they compared SWE values from the CRS to manual snow survey and snow stake measurements and found that the sensor was able to accurately measure up to 56 cm of water equivalent with a precision better

than 1 mm for water-equivalent thicknesses less than 14 cm and better than 1 cm in up to 140 cm, or approximately 0.7% (Howat et al., 2018).

Overall, all of these results indicate that with additional research confirming the applicability of CRSs at different sites, the use of neutron detection as a form of continuous snow monitoring has significant potential to become a vital approach in modern snow measurement techniques.

2. GROUND-BASED COSMIC RAY SENSORS FOR THE CONTINUOUS MEASUREMENT OF ARCTIC SNOW ACCUMULATION AND MELT

Jitnikovitch A[1]., Marsh P[1]., Walker B[1]., and Desilets D[2].

[1]Cold Regions Research Centre, Wilfrid Laurier University, Waterloo, ON, Canada

[2]Hydroinnova LLC, Albuquerque, NM, United States of America

Abstract

The Arctic is warming at twice the rate of the global average, causing a significant impact on snow accumulation and melt. Unfortunately, standard methods to measure snow water equivalent (SWE) have numerous limitations which hinder our ability to document snow cover conditions or to test predictive models. As a result, there is an urgent need for improved methods which measure snow on the ground and allow for continuous measurements over spatially variable snow covers. Cosmic ray sensors (CRSs) may fill this observational gap, but few studies have tested these types of sensors, and none have considered their applicability in the continental Arctic. We test a ground-based CRS at two locations, a high-SWE environment in the Canadian Arctic and a low-SWE landscape near Elora, Ontario. CRS moderated neutron counts were compared to manual snow survey SWE values obtained during field seasons. Pearson correlation coefficients range from -0.89 to -0.98, while regression analyses provided R^2 values from 0.79 to 0.96. It was found that the ground-based CRS has the potential to continuously measure SWE in remote regions and in variable topography. Such continuous SWE measurements have important applications for testing snow and hydrological models, flood risk-assessments and water resource management.

Keywords: Arctic, snow water equivalent, cosmic ray sensors, neutrons

2.1 Introduction

Snow on the ground is a keystone property of the Arctic and has a significant impact on the interactions among climate, permafrost, vegetation, animals, streamflow, lake levels, lake ice, aquatic ecology, and northern infrastructure. As the climate has changed over the last 50 years (ACIA, 2005; Qu and Hall, 2006; Tollefson, 2017), the number of weeks with snow on the ground across the Arctic has declined considerably (Derksen and Brown, 2012; Rees et al., 2014; Hori et al., 2017; NSIDC, 2017), but changes to other aspects of the snow environment have not been well documented. For example, the effects of a changing climate on snowfall, mid-winter thaws, blowing snow, expanding shrubs capturing blowing snow, spatial variability in snow depth and snow water equivalent (SWE), and the rate of spring melt are poorly known. Although there are various ongoing international efforts to expand Arctic observing networks in order to better document ongoing changes to the Arctic environment (Schiermeier, 2006; Goodsite et al., 2016; CNNRO, 2016), efforts to monitor snow are severely limited by deficiencies in our ground-based methods to measure snow on the ground. The following will discuss efforts to improve ground-based observations of snow, including both manual observations and instruments, but will not consider airborne or satellite based remote sensing issues (Seidel and Matinec, 2004; Takala et al., 2011)

Deficiencies in ground-based snow observations are due to the combined effects of the small number of observation stations across the vast Arctic (Schiermeier, 2006; Rees et al., 2014; Goodsite et al., 2016) and large errors and limitations in ground-based techniques (Goodison et al., 1981, Pomeroy and Gray, 1995; Kinar and Pomeroy, 2015; Wrona, 2016). For example, accurately sampling deep snow drifts that are scattered across the landscape is extremely challenging, but essential for quantifying snow on the ground across complex Arctic landscapes.

An indication of the importance of drifts is noted in previous studies which estimated that snow drifts account for up to 70% of the total winter snowfall in many areas of the Arctic (Gray et al., 1974; Marsh and Woo, 1981; Gray et al., 1989). However, sampling slope and vegetation-controlled drifts across large regions is very difficult, and current estimates of the amount of snow contained in drifts are expected to have large errors. In addition, manually probing snow that is up to 10 meters in depth and of very high-density, is often impossible and dangerous if they are located on steep slopes. It is also important to note that manual snow surveying during blowing snow events are not possible, and as a result, there is limited data on blowing snow accumulation during individual events as required for testing blowing snow models. Ground-based instruments for measuring snow are also prone to significant problems. For example, ultrasonic systems commonly have significant errors in measuring snow depth due to temperature, winds, and when measuring soft or irregular surfaces (Kinar and Pomeroy, 2007); ground-based LIDAR systems also have errors in measuring snow depth over complex terrains and forested sites (Deems et al., 2013); while gamma-based sensors provide continuous point measurements of SWE, but have limited ability to measure deep snowpacks (Paquet et al., 2008). In addition, all of these systems are typically limited to point measurements that can not provide information on the large variability in snow depth, density and SWE that is typical over small horizontal distances in the Arctic.

Cosmic ray sensors (CRS) (Desilets et al., 2010; Zreda et al., 2012; Sigouin and Si, 2016; Schattan et al., 2017) offer another instrumentation option that has potential to fill many of the gaps conventional methods have. CRSs can measure a point estimation of SWE, or alternatively, an areal average of SWE (depending on the type of CRS) due to the attenuation of incoming cosmic rays. Kodama et al. (1979) first utilized cosmic rays to measure SWE by burying a

shielded neutron sensor below the ground surface and allowing snow to accumulate upon it. This method records neutrons in the fast to epithermal range (Kodama et al., 1979; Zreda et al., 2008), which are guided along Earth's magnetic field and are attenuated by hydrogen atoms in the snow, weakening its energy level with every collision until it is at an appropriate energy level (~1 MeV or less) to penetrate the instrument casing (shield) and be recorded as a neutron count. The neutron counts are inversely related to the amount of SWE on the ground due to the neutron moderating characteristic of hydrogen. Due to this, the CRS instrument measurements do not discriminate towards wet snow, ice lenses, or dry snow; a prominent advantage over current methods. Kodama et al. (1979) showed a strong negative correlation between moderated neutron counts and SWE, however, due to the configuration of the neutron sensor used in that study, only a small SWE could be recorded. More recently, Hydroinnova developed a CRS to measure soil moisture (Desilets and Zreda, 2003; Zreda et al., 2012; Chrisman and Zreda, 2013; Rosolem et al., 2013; Coopersmith et al., 2014; Köhli et al., 2015; Wrona, 2016), these were installed in a network consisting of over 48 instrumented sites. Due to the design of these sensors, they also have the potential to measure SWE (Desilets et al., 2010; Rasmussen et al., 2012; Sigouin and Si, 2016; Schattan et al., 2017; Howat et al., 2018). Another prominent network of CRSs is located in the French Alps, Pyrenees and Massif Central where Électricité de France (EDF) has deployed 40 ground-based instruments (Paquet et al., 2008; Zreda et al., 2012; Delunel et al., 2014). EDF designed this network to measure winter snow cover in order to estimate snowmelt runoff to hydroelectric power plants. These existing CRS networks indicate the potential for an improved method to measure SWE remotely, continuously, and across a range of landscapes.

Given the prominent deficiencies in available instruments to continuously measure accumulation of SWE across Arctic landscapes where snow is extremely shallow in wind

scoured regions, but many meters in depth in snow accumulation zones, this paper has the primary objective of testing a ground-based CRS, developed by Hydroinnova and called the SnowFox (SF), for measuring SWE across large snow drifts, and will make recommendations for developing appropriate Arctic observing systems. Such improved measurement methods of SWE across the Arctic will enhance flood forecasting, water resource management, ecological knowledge (Liston et al., 2016), remote sensing and hydrological modeling (Goodison et al., 1987; Kinar and Pomeroy, 2015).

2.2 Study Sites

Field observations using the ground-based CRS were conducted in both northern and southern Canada over the 2016/17 and 2017/18 winters. This allowed testing during two winter seasons and over a range of environmental conditions. These sites include the following:

2.2.1 Trail Valley Creek, Northwest Territories

The Arctic field site is located in Trail Valley Creek (TVC) (68.4 ˚N, 133.3 ˚W), 50 km north of Inuvik, Northwest Territories, Canada. Six ground-based CRSs were installed along a 50 m transect that traversed from a tundra landscape and across an alder shrub patch (alders are up to 1.5 m in height), with each CRS placed on the ground surface prior to the accumulation of snow. For this installation, the six CRSs were installed approximately 8 m apart (Fig. 2.1), and connected to a single data logger. This shrub patch accumulates a large snowdrift each winter and represents a typical high-SWE Arctic environment. Unfortunately, the CRS at the northern margin of this transect (SF6 from Fig. 2.1) failed prior to the start of the experiment and was excluded from this study, in addition, the CRS system experienced power failure in the 2017/18 winter season from November 10 to 27, 2017. This CRS network was installed on August 5, 2016 and remained in place for both the 2016/17 and 2017/18 winter seasons.

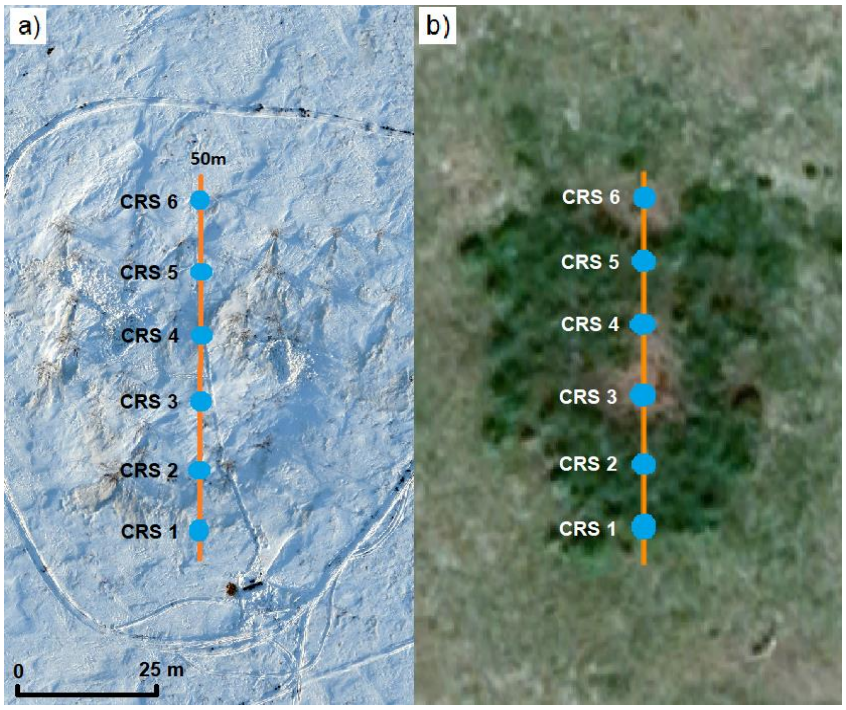

Figure 2.1. Ground-based CRSs (blue dots) at the TVC site during the 2016/17 and 2017/18 field seasons**.** Orange line represents the snow survey transect conducted at this site. **a)** Image was taken with a high-resolution unmanned aerial vehicle displaying a snow-covered site. **b)** Image is from Google Earth (July 2018) displaying a snow-free site, dark green vegetation are alders while light green is typical tundra vegetation.

2.2.2 Elora, Ontario

A field site outside of Waterloo, Ontario was also instrumented in order to test the ground-based CRS in a temperate environment. This field site is located in Elora, Ontario in an agricultural field (43.6˚N, 80.3˚W) (Fig. 2.1) and 30 km from Wilfrid Laurier University. This site typically has a shallow snow cover, low-SWE snowpack, with minimal spatial variability in SWE. The CRS was placed in the centre of this field and was representative of an open-area landscape which is impacted by natural factors such as wind and sublimation. This field was tilled before the sole ground-based CRS was installed on February 11, 2017 for the 2016/2017

winter season and on December 5, 2017 for the 2017/2018 winter season. Unfortunately, the CRS experienced a power failure and did not record data from January 13 to 23, 2018.

Figure 2.2. Location of ground-based CRS (noted by blue dot) at the Elora site during the 2016/17 and 2017/18 winter field seasons.

2.3 Methods

2.3.1 Hydroinnova ground-based CRS

The Hydroinnova CRS we are using in this work is a ground-based CRS called the SnowFox (SF). This instrument possesses a single sensor tube, located at the snow-ground interface and provides point observations (1 m^2) of SWE. These ground-based CRSs can be used individually, or a number of sensors can be connected to a single data logger to provide measurements along a transect of several hundred meters in length. Using multiple CRSs along a

transect provides a unique capability to continuously measure SWE over an entire winter, including under blowing snow events and across challenging terrains such as vegetation patches, ridges, hills, and mountain overhangs. The ground-based CRS measures moderated neutrons and has only had very limited field testing (Howat et al., 2018). Although snowdrifts are often extremely deep and account for large proportions of meltwater, the accurate measurement of these drifts is difficult using snow probing methods during snow surveys (Marsh and Woo, 1981; Gray et al., 1989). The ground-based CRS has significant promise to fill this measurement gap by providing continuous readings, including during precipitation and blowing snow events. In addition, the CRS is appealing for SWE measurements because it does not require any physical maintenance (other than batteries), is terrain independent, can be set up by a single person in under an hour, and has a low environmental impact as it does not require anti-freeze coolant (unlike snow pillows). Additionally, it has capabilities to measure at least 4 meters and potentially up to 10 meters of SWE (Howat et al., 2018), more than any practical SWE measurement device.

The ground-based CRS sensor is a 130 cm cylindrical detector tube with a control module incorporating a Hydroinnova QDL2100 data logger as well as an iridium satellite communication device. The detector tube contains ^{3}He gas, this gas is used due to its stability. The detector tube is considered moderated (shielded) due to its polyethylene and lead casing and measures high energy neutrons (~1 MeV or less) which traverse through the snowpack and are attenuated by hydrogen. It is important to note that prior to hydrogen attenuation these neutrons are considered to be of an extremely high energy (larger than 1 MeV). As these neutrons attenuate to an energy level of ~1 MeV and collide with the CRS instrument, they penetrate the polyethylene and lead casing causing the high energy of the neutron to be reduced to about 1/40th

of an electron volt. At this point, a helium atom in the detector tube absorbs the neutron and splits into a lithium ion. These ions remove electrons from neutral atoms in the detector tube and produce a charge in the tube of gas. These newly charged ions are then detected and amplified by a built-in amplifier inside the CRS. The sensor then records this as 1 neutron count (Bartol, 1999). This process continues over the pre-set measurement interval (also known as the neutron intensity), and is automatically posted in real-time on a private web portal provided by Hydroinnova.

2.3.2 Determination of Corrected Neutron Counts

Before the neutron intensity data can be analysed to consider SWE, the raw moderated neutron counts must be corrected for differences in the barometric factor (F_p) and the temporal variation of incoming cosmic rays (F_i) as outlined in the equations below (Desilets, 2017). Since these correction factors (F_p and F_i) represent a change from one point in time to another, they are unitless.

$$N_{COR} = N_{RAW} \times F_p \times F_i \quad \textbf{(2.1)}$$

The corrected moderated neutron counts (N_{COR}) is calculated as a function of the raw moderated neutron counts (N_{RAW}) as recorded by the CRS data logger, and are also available on a private web portal provided by Hydroinnova. N_{COR} (moderated neutron counts per hour) is corrected for the change in barometric pressure (F_p), which influences the attenuation of the cosmic ray flux as it moves through the atmosphere and the temporal variation in incoming cosmic rays (F_i).

F_p is calculated as:

$$F_p = e\left(\frac{P-P0}{L}\right) \quad \textbf{(2.2)}$$

where e is the natural exponential, P is the observed air pressure (hPa) recorded by a pressure sensor on the CRS instrument. P_0 represents a reference air pressure, set to 1000 hPa (as recommended by Hydroinnova) and L is the mass attenuation length (cm) (Tables 1 and 2) and was also provided by Hydroinnova. F_i is then calculated as:

$$F_i = N_{avg}/N_{nm} \quad \textbf{(2.3)}$$

where N_{avg} is the average neutron monitor count rate for the study period and N_{nm} is the hourly neutron count during the time of interest. Several studies which tested an above-ground CRS model (Zreda et al., 2012; Chrisman and Zreda, 2013; Schattan et al., 2017) use cosmic ray fluxes from the Jungfraujoch Neutron Monitor in Switzerland. However, given the effect of the Earth's magnetic field, and therefore latitude, on incoming cosmic ray flux, in this paper we will use cosmic ray fluxes from the neutron monitor at the Aurora Research Institute, Inuvik, NWT, and available from the Neutron Monitor Database (www.nmdb.eu). This station is located 50 km south of the TVC study site, and at approximately the same elevation.

N_{COR} from equation 2.1 was then averaged over a 12-h period in order to reduce the noise associated with the hourly moderated neutron data and is represented as N. Findings from Schattan et al. (2017) state that averaging the raw moderated neutron count is vital since using hourly values can translate into errors of up to 40%, while using 12-h averaged data reduces the

uncertainty of estimating SWE to a value of 1-12%, with an average of 4%. This also leads to a reduction in measurement uncertainty while being sensitive enough to respond to low and moderate snow accumulation/erosion events (either due to snowfall or blowing snow) (Zreda et al., 2008).

Finally, N was converted into SWE (mm) as follows (personal communication with Hydroinnova, NM, USA, May 19, 2017):

$$\mathrm{SWE} = -10 \times \left(\frac{1}{\frac{1}{L}}\right) \times \ln\left(\frac{N}{\mathrm{N0}}\right) \quad \textbf{(2.4)}$$

where ln is the natural logarithm, N is the corrected and 12-h averaged moderated neutron count, and N_0 represents the averaged neutron count 7-14 days prior to the initial snow precipitation of the season (this serves as the instrument's moderated neutron count baseline). L, the mass attenuation length (cm) (Tables 1 and 2) is then calculated as:

$$\frac{1}{L} = \frac{1}{L}\mathrm{max} + \left(\frac{1}{L}\mathrm{min} - \frac{1}{L}\mathrm{max}\right) \,/\, (1 + e\left(-\frac{\left(\frac{\mathrm{N}}{\mathrm{N0}-\mathrm{a1}}\right)}{\mathrm{a2}}\right))^{\mathrm{a3}} \quad \textbf{(2.5)}$$

Parameter values for Lmax, Lmin, a1, a2 and a3 are found in Tables 2.1 and 2.2.

Desilets (2017) provides two sets of parameters based on technical studies while developing the CRS instrument. The standard terrestrial parameters (Table 1) were used for the Elora study site. However, as the TVC snow cover was underlain by a high porosity soil matrix that is typically saturated with liquid water prior to freeze up, and therefore ice during the winter

(Wrona, 2016), we applied Desilets (2017) glacier parameters (Table 2) to the TVC site. In addition, the a1 parameter was slightly increased by systematic trial-and-error, in order to address the factor that the TVC subsurface was not pure water/ice, but had mineral and organic properties as well. Please note that the Lmax value represents the rapid attenuation of fast neutrons while the Lmin value represents a more gradual attenuation. Parameters a1, a2 and a3 are best fit parameters and were obtained by trail-and-error (personal communication with Hydroinnova, NM, USA, October 27, 2018).

Table 2.1. Parameters used for the Elora site. Values were obtained from Hydroinnova and are representative of a terrestrial landscape.

Elora	
Parameter	Value
Lmax	134.7
Lmin	20
a1	0.612
a2	0.073
a3	0.598

Table 2.2. Parameters used for the Trail Valley Creek shrub site. Values were obtained from Hydroinnova and are representative of a glacier landscape. NOTE: a1 parameter was changed from 0.313 to 0.355 to represent the high porosity, saturated soils of the study site.

Trail Valley Creek	
Parameter	Value
Lmax	114.4
Lmin	14.1
a1	0.355
a2	0.083
a3	1.117

2.3.3 Snow Surveys and Application of Data

2.3.3.1 Elora, Ontario

Snow surveys were performed at the Elora site over the 2016/2017 and 2017/2018 field seasons. In the 2016/2017 season, a total of 5 snow surveys were conducted during melt and non-melt conditions from February 11, 2017 to March 14, 2017. In the 2017/2018 season, a total of 13 surveys were conducted from December 23, 2017 to February 20, 2018. Unfortunately, the CRS suffered a power failure and did not record data from January 13 to 23, 2018, and as a result, snow survey data from January 17, 2018 and January 19, 2018 was excluded from this analysis. Therefore 11 snow survey measurements were used for the 2017/18 winter season. Snow surveys consisted of three to four snow core samples taken within a 1 m proximity to the ground-based CRS. Snow survey values were then averaged to represent a single value for that date. Snow core samples were collected with a SnowHydro snow tube with a cross sectional area of 30 cm^2. The snow cores were transferred to a plastic bag and weighed on-site with an electronic scale (A&D HT-3000). The depth and density of each snow sample was recorded and used to calculate SWE.

2.3.3.2 Trail Valley Creek, Northwest Territories

Snow surveys were performed at TVC during the 2016/2017 season from December 13, 2016 to June 6, 2017 and April 28, 2018 to June 7, 2018 during the 2017/2018 season. 17 snow surveys were conducted in 2016/17 and 28 in the 2017/18 winter season. The snow surveys included melt and non-melt conditions and consisted of 10 measurements (approximately equally spaced apart) along a 50 m transect. Again, a SnowHydro snow tube was used. Using the same approach as the Elora site, all samples had their depth and weight recorded on-site and were used to calculate SWE. Snow survey data from this site was used in two ways,

1) SWE calculated from the 5 ground-based CRSs was averaged and this single value was used to represent the total snowdrift for that date.
2) SWE calculated for each CRS was compared with the snow survey measurement obtained nearest to the specific CRS of interest. This allowed the CRSs to be compared to one-another within the snowdrift over the course of the winter season.

It is important to note that the CRS experienced a power failure from November 10 to 27, 2017, during the 2017/18 winter season.

2.4 Results and Discussion

2.4.1 Relationship between Neutron Counts and Physical Snow Properties

2.4.1.1. Moderated neutron counts and snow density and depth

Since moderated neutron counts are directly affected by hydrogen, it is expected that the moderated neutron counts should be most sensitive to SWE (which is a combination of depth and density), however, it is important to consider the relationship between moderated neutron counts and depth and density independently in order to obtain a detailed analysis of the root variables that make up SWE. For the Elora site, non-melt (non-zero) snow density ranges from 74 kg/m^3 to 332 kg/m^3 (Fig. 2.3a) with a standard deviation (STDEV) ranging from 7 kg/m^3 to 50 kg/m^3. The Pearson correlation coefficients between neutron intensity and density were found to be -0.88 and -0.76 for each year, while the R^2 values were 0.77 and 0.58. Separately, when comparing the neutron intensity to depth (Fig. 2.3b), non-melt values have a depth range between 6 cm and 22 cm with a STDEV ranging from 1 cm to 3 cm. The Pearson correlation coefficients between the neutron intensity and depth were found to be -0.70 and -0.83, while the R^2 values were noted as 0.49 and 0.68 in the 2016/17 and 2017/18 winter seasons respectively. These high associations indicate a strong relationship between each pair of variables. Ultimately, these relationships

show that an increase in snow density/depth leads to a decrease in neutron intensity (as shown by the negative Pearson correlation values and negative sloping trend lines in Fig. 2.3ab). This is explained by noting that snow density typically increases with snow depth (and vice versa). As snow accumulates, the overlying snow compacts the grains below it, increasing the density, and in turn, decreasing the neutron intensity due to an increased attenuation by hydrogen atoms (Desilets et al., 2010; Siguoin and Si, 2016; Schattan et al., 2017; Howat et al., 2018).

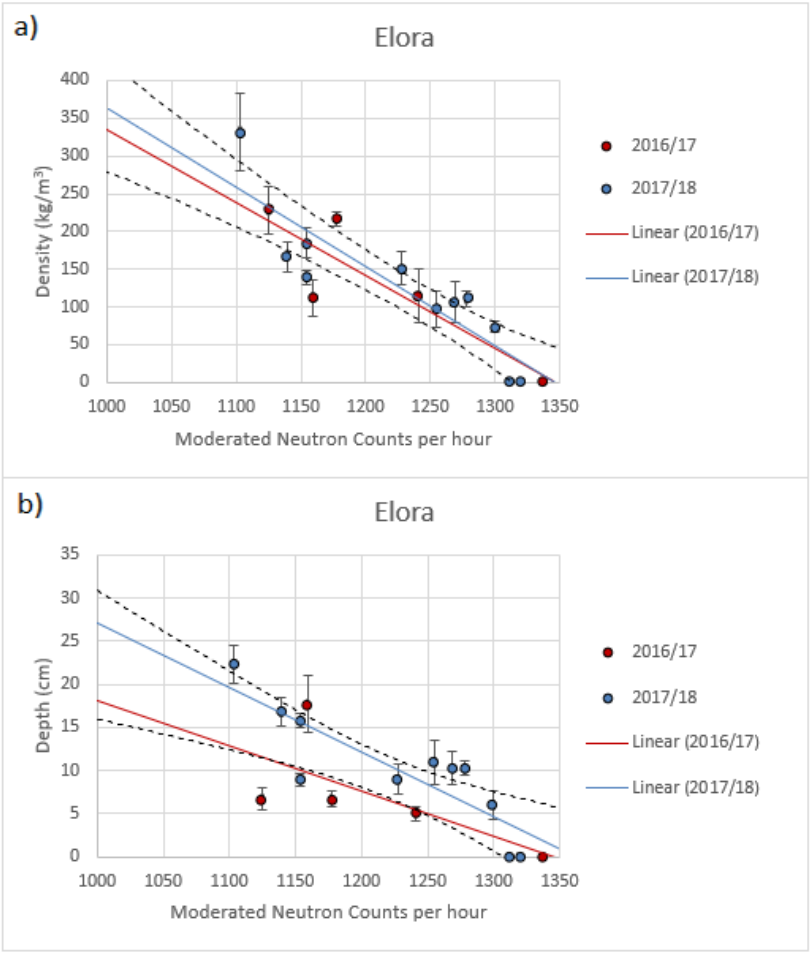

Figure 2.3. a) 2016/17 and 2017/18 neutron counts per hour vs. density and **b)** 2016/17 and 2017/18 neutron counts per hour vs. depth at the low-SWE Elora site. Each density/depth point is from an averaged snow survey and is corresponded to a 12-h averaged neutron intensity measured by the CRS on the same date. Please note that the zero depth/density values represent melt conditions and the error bars represent the standard deviations. The dashed lines represent a 95% confidence interval.

From the TVC site, non-melt (non-zero) values have a density range from 71 kg/m^3 to 429 kg/m^3 (Fig. 2.4a) with a STDEV ranging from 24 kg/m^3 to 200 kg/m^3. The Pearson correlation coefficients between the neutron intensity and density were found to be -0.71 and -0.85, while the R^2 values were determined to be 0.51 and 0.72 in 2016/17 and 2017/18 respectively. Interestingly, the strength of the relationship between density and neutron intensity for 2016/17 is considerably lower than for 2017/18. This is likely explained by noting the large range of neutron intensities and densities associated with the corresponding snow samples obtained in 2016/17 in comparison to 2017/18 (Fig. 2.4a). Separately, when comparing the neutron intensity to depth (Fig. 2.4b), non-melt values have a depth range between 2 cm and 116 cm with a STDEV ranging from 3 cm to 44 cm. The Pearson correlation coefficient was -0.95 and -0.86, with R^2 values of 0.91 and 0.74 in the 2016/17 and 2017/18 winter seasons respectively. Once again, these associations indicate that a strong relationship exists between the variables and that there is a strong potential to predict future depth values at this site. Similar to results found at the low-SWE, Elora site (Fig. 2.3), an increase in density/depth at TVC was found to cause a decrease in the moderated neutron count (as shown by the negative Pearson correlation values and negative sloping trend lines in Fig 2.4ab).

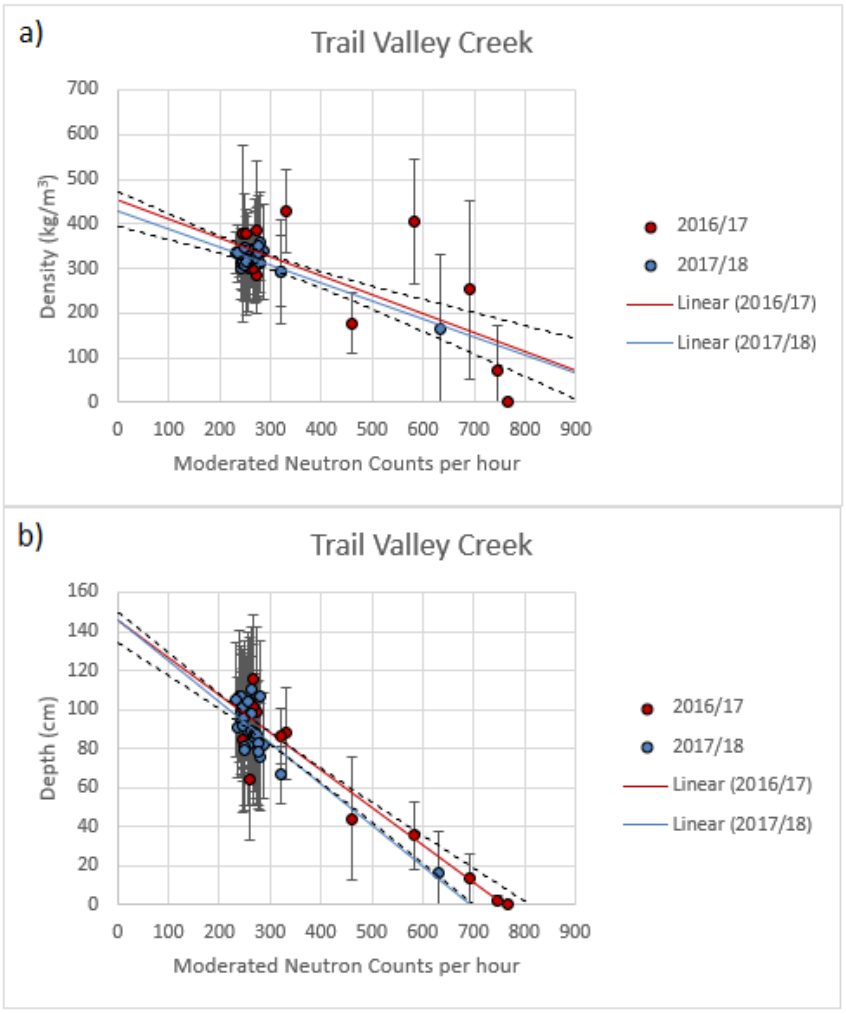

Figure 2.4. a) 2016/17 and 2017/18 neutron counts per hour vs. density at the high-SWE, TVC site and **b)** 2016/17 and 2017/18 neutron counts per hour vs. depth at the high-SWE, TVC site. Each density/depth point is from an averaged snow survey and is corresponded to a 12-h averaged neutron intensity measured by the CRS on the same date. Please note that the zero depth/density values represent melt conditions and the error bars represent the standard deviations. The dashed lines represent a 95% confidence interval.

2.4.1.2. Moderated neutron counts and SWE

In the section above, we considered the relationship between moderated neutron counts and both snow depth and density independently. However, from the theory on which the cosmic ray sensors are based, the decrease in neutron counts is directly related to the interactions with hydrogen, and therefore the strongest relationship should be between neutron counts and SWE.

This section will analyse this relationship, while the following (*2.4.1.3)* will summarize all three relationships.

Moderated neutron counts were assessed in relation to SWE at both sites during both years, with the goal of creating an empirical formula which can, in some cases, be used to predict SWE. We recommend using these equations only when the user is interested to quickly estimate a reasonable potential amount of SWE at the specific site the ground-based CRS was corrected for. It is important to note that the longer duration the empirical formulas are used in a season, the larger margin of error they output and the more unreliable their results become. This is because these equations are only directly representative of the seasonal dynamics involved during their specific winter season. Additionally, they do not directly incorporate significant variables such as the barometric pressure or the temporal cosmic ray flux which have potential to vary considerably over short and/or long timeframes. ANOVA tables and summary statistics from the regressions conducted in this section (*2.4.1.2*) can be found in Appendix B (Tables B.5. to B.12.).

To assess the low-SWE, Elora site, a bivariate analysis and a simple linear regression between the 12-h averaged moderated neutron intensity recorded by the CRS and the averaged SWE from snow surveys was conducted (Fig. 2.5a). The STDEV of SWE for the snow surveys ranged from 1 cm to 11 cm and had Pearson correlation coefficients of -0.95 for 2016/17 and -0.97 for 2017/18, with R^2 values of 0.92 and 0.94 for 2016/17 and 2017/18.

The empirical equations were determined to be:

$$SWE_{Elora2016/17} = -0.084(N) + 112.0 \quad \textbf{(2.6)}$$

and

$$SWE_{Elora2017/18} = -0.144(N) + 191.9 \quad \textbf{(2.7)}$$

Where N is the 12-h averaged moderated neutron count which is corrected for changes in barometric pressure (F_p), and the incoming temporal cosmic ray flux (F_i). The RMSE of the CRS-measured SWE was 1.8 mm in 2016/17 and 2.3 mm in 2017/18.

When examining equations 2.6 and 2.7, it is clear that the slope and y-intercept values are considerably different from year-to-year. This discrepancy in the y-intercept can be related to the CRS being installed near the end of the winter season (February 11, 2017) in 2016/17 and therefore the instrument baseline did not incorporate the water content in the first few centimeters of soil - where the CRS experiences back scattering of neutrons (Zreda et al., 2008; Desilets et al., 2010; Siguoin and Si, 2016). This baseline (N_0) is incorporated by averaging the moderated neutron count 7-14 days prior to the initial snow precipitation of the season. On the other hand, the CRS during the 2017/18 season was installed on December 4, 2017, before the first snow-precipitation of the season and before the initial soil freeze-up. This means the CRS's baseline between the two seasons are considerably different. To adjust for this, it was estimated that 5 mm of antecedent water was stored in the first few centimeters of soil during the 2016/17 winter season. This value was chosen because for this type of soil, water capacity could range from 1.3 to 2 mm/cm (Blencowe, 1960; Ball, 2001). In order to illustrate the possible effect of soil water on the CRS readings, we assumed a 50% soil moisture. This 5 mm value was added to all non-melt (non-zero) SWE values from snow surveys conducted in 2016/17 and a linear regression was repeated (Fig 2.5b). A similar approach was conducted by Sigouin and Si (2016) where they estimated soil water storage in the top 10 cm of the soil profile and added it to their

SWE values in the corresponding year. After implementing these changes and conducting a second regression to the 2016/17 data, the equation became:

$$SWE_{Elora2016/17adjusted} = -0.107(N_{COR}) + 143.9 \quad \textbf{(2.8)}$$

When comparing the original 2016/17 empirical formula to the adjusted one (equations 2.6 and 2.8), it is clear that both the slope and y-intercept values increased and shifted considerably closer to the slope and y-intercept values of the 2017/18 equation (equation 2.7). The adjusted 2016/17 data yields an improved Pearson correlation coefficient of -0.98, an improved R^2 value of 0.96 and a slightly lower RMSE of 1.7 mm.

Figure 2.5a displays the 2016/17, 2017/18 and both years combined data for Elora while Figure 2.5b displays the same data but with the 2016/17 values adjusted for the estimated antecedent soil water content. The R^2 value of the combined regression is 0.89, a considerable improvement from the original (pre-adjusted SWE values for Elora, 2016/17) combined R^2 value of 0.77. The similarity of trend lines at Elora in 2016/17 and 2017/18, displays the consistency of the CRS when measuring SWE in a low-SWE environment.

It is interesting to note, Kodama et al. (1979) used an exponential curve rather than a linear one to estimate SWE from the moderated neutron intensity, this approach was tested in this research. Prior to conducting an exponential curve, all 0 values had to be changed to reflect non-zero values, as a result, these values were altered to 0.01 mm of SWE. An exponential regression was then conducted and yielded an R^2 value of 0.55. Since this value is considerably lower than both the original and adjusted Elora R^2, it was discarded and a linear regression was chosen to estimate SWE at this site for future purposes.

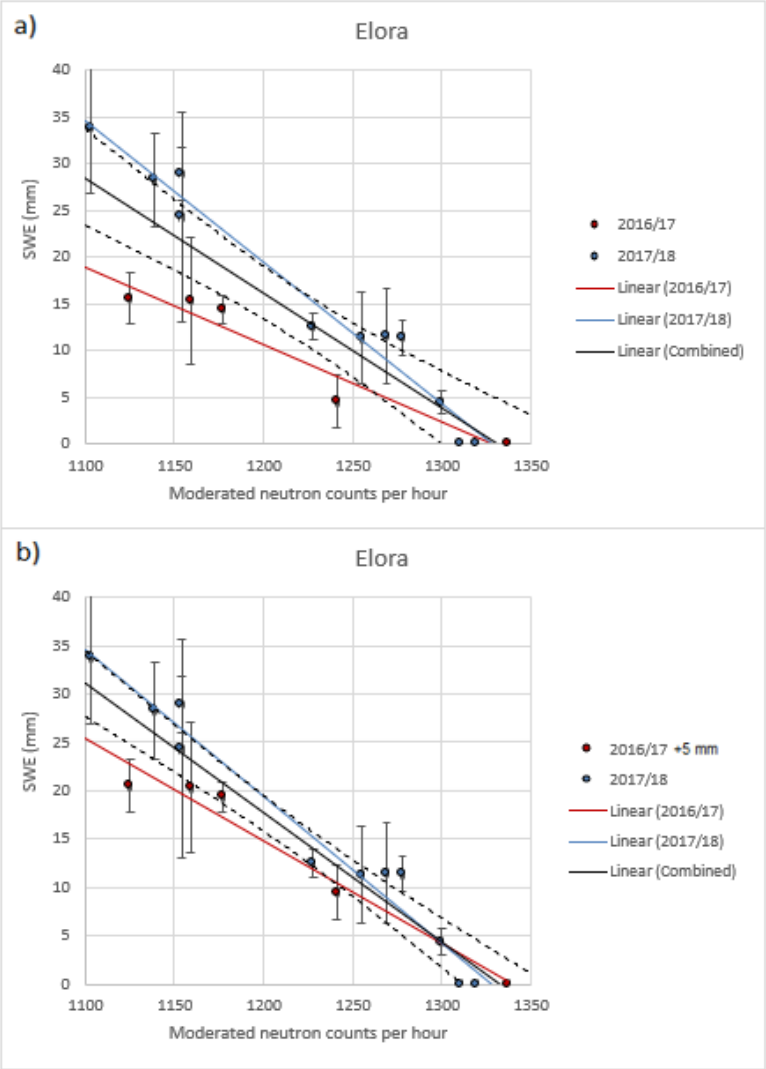

Figure 2.5. a) 2016/17 and 2017/18 SWE vs moderated neutron counts per hour and **b)** 2016/17 and 2017/18 SWE vs moderated neutron counts per hour at the low-SWE, Elora site, however, 2016/17 SWE values are adjusted to account for the antecedent water content in the top few centimeters of soil. Each SWE point is from an averaged snow survey and corresponded to a 12-h averaged neutron intensity measured by the CRS on the same date. Please note that the zero SWE values represent melt conditions and the error bars represent the standard deviations. The dashed lines represent a 95% confidence interval.

The same analysis procedure was repeated for the high-SWE, TVC site. A bivariate analysis and a simple linear regression was conducted on the CRS transect 12-h averaged moderated neutron intensity and averaged SWE measurements from snow surveys (Fig. 2.6).

The STDEV of SWE for the snow surveys ranged from 11 mm to 184 mm. For 2016/17, the Pearson correlation coefficient was determined to be -0.95, with an R^2 value of 0.91, indicating that 91% of the variance of SWE can be explained by the associated moderated neutron count.

The empirical equation was determined to be:

$$SWE_{TVC2016/17} = -0.679(N) + 515.1 \quad \textbf{(2.9)}$$

where N is the 12-h averaged moderated neutron count which is corrected for changes in barometric pressure (F_p), and the incoming temporal cosmic ray flux (F_i). The CRS-measured SWE was similar to that of the snow surveys and had a RMSE of 39.6 mm.

An analysis was conducted on the 2017/18 TVC data. The STDEV of SWE for the snow surveys ranged from 67 mm to 160 mm. The Pearson correlation was determined to be -0.89 with an R^2 value of 0.79. Although weaker than the Pearson correlation value found for 2016/17, it is still representative of a very strong correlation. The empirical equation was determined to be:

$$SWE_{TVC2017/18} = -0.715(N) + 500.9 \quad \textbf{(2.10)}$$

The CRS-measured SWE was similar to that of the snow surveys and had a RMSE of 27.8 mm.

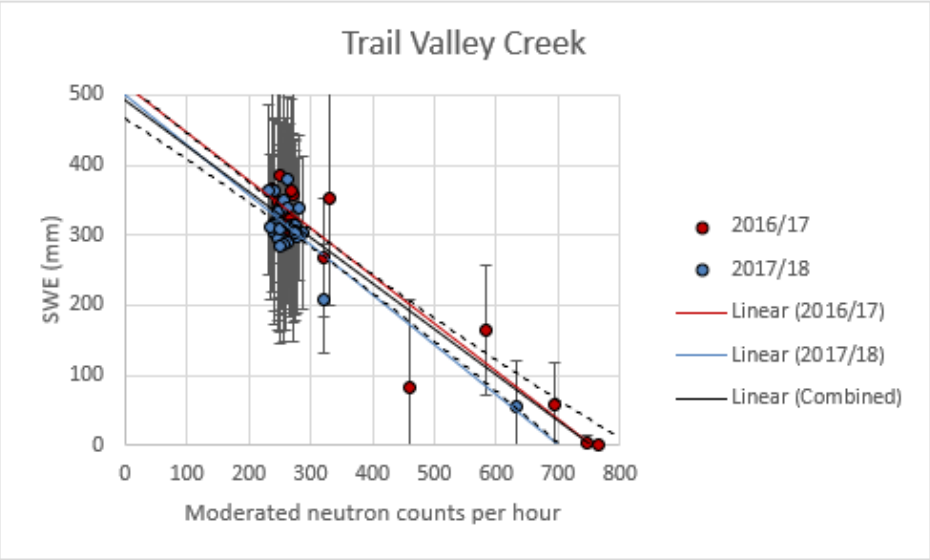

Figure 2.6. 2016/17 and 2017/18 SWE vs moderated neutron counts per hour at the high-SWE, TVC site. Each SWE point is from an averaged snow survey and corresponded to a 12-h averaged neutron intensity measured by the CRS on the same date. Please note that the zero SWE values represent melt conditions and the error bars represent the standard deviations. Also, please note the scale difference between Figure 2.5 and 2.6. The dashed lines represent a 95% confidence interval.

2.4.1.3. Comparison of relationship between moderated neutron counts and depth/density, SWE

When assessing Table 2.3, it is clear that the relationship between the neutron intensity and depth/density is weaker than the relationship between neutron intensity and SWE. This trend is noted for both sites and both years. Not surprisingly, the weakest relationship was noted between the moderated neutron count and density since it displayed the most variability from year-to-year at both sites. The relationship between the neutron intensity and depth was found to be stronger but still displayed some variability year-to-year at both sites. As expected, the strongest relationship found at both sites and years was between the moderated neutron count and SWE. This relationship is directly related to the increased presence of hydrogen atoms as SWE accumulates, effectively increasing the attenuation of cosmic rays as they traverse through the snowpack.

Table 2.3. Pearson correlation coefficients (*r)* and coefficients of determination (R^2) summary table.

	Elora – Depth	Elora – Density	Elora – SWE	TVC – Depth	TVC – Density	TVC – SWE
2016/17	*r*= -0.70 R^2= 0.49	*r*= -0.88 R^2= 0.77	*r*= -0.98 R^2= 0.96	*r*= -0.95 R^2= 0.91	*r*= -0.71 R^2= 0.51	*r*= -0.95 R^2= 0.91
2017/18	*r*= -0.83 R^2= 0.68	*r*= -0.76 R^2= 0.58	*r*= -0.97 R^2= 0.94	*r*= -0.86 R^2= 0.74	*r*= -0.85 R^2= 0.72	*r*= -0.89 R^2= 0.79

2.4.1.4. Summation of in-situ snow core sampling and corresponding CRS-measurements

Figure 2.7 displays the averaged snow survey sampling SWE and the corresponding CRS SWE-measurements from the 2016/17 and 2017/18 winter field seasons at the low-SWE (Elora) and high-SWE (TVC) sites. CRS SWE data in Elora is from 1 ground-based sensor while TVC data is averaged from 5 ground-based sensors. Both sites and years used equation *2.4* to determine the CRS-measured SWE. Since we are comparing the SWE from manual snow surveys to the CRS-measured SWE, a type II linear regression was conducted on the combined data. This presented an almost linear slope of 0.95 and an R^2 value of 0.96. Admittedly, it would be beneficial to have additional measurements in the 100-300 mm range, but the measurements produced by the CRS still correlate very well over the broad range of SWE values from both sites and years. This further indicates the sensor's ability to provide accurate measurements at both a low-SWE (Elora) and high-SWE (TVC) environment.

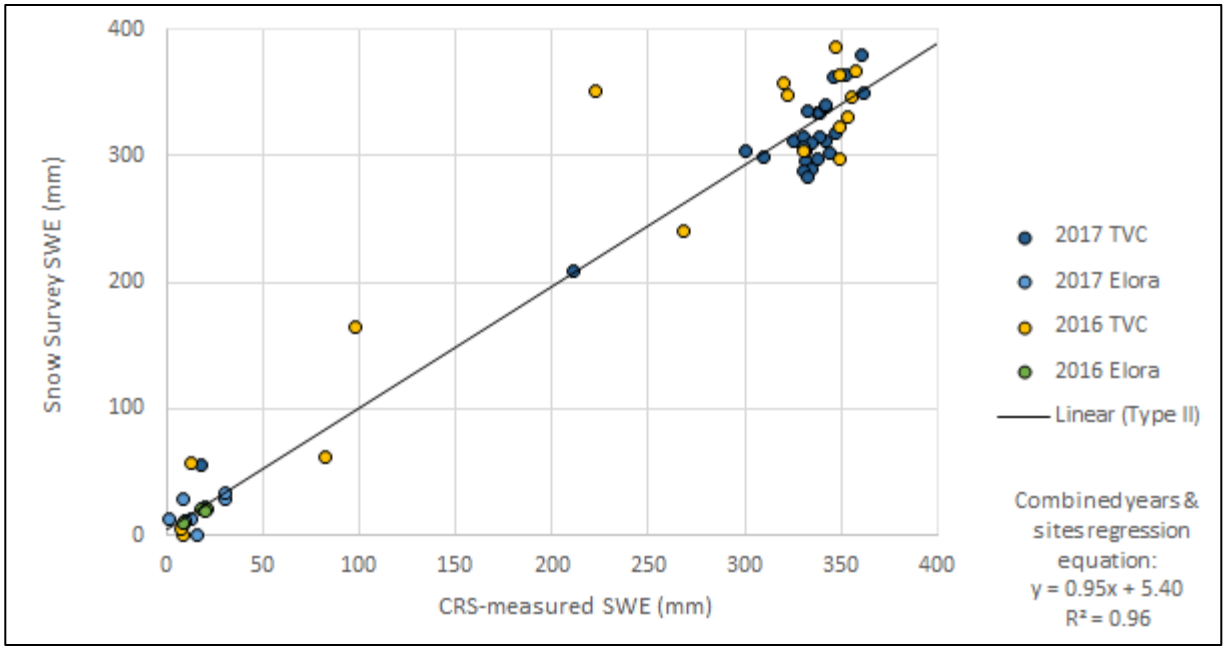

Figure 2.7. Comparison between averaged on-site core samplings and averaged ground-based CRS measurements during the 2016/17 and 2017/18 field seasons at the Elora and Trail Valley Creek sites.

2.4.2 Application of the ground-based CRS for Continuous Measurement of SWE at a Point

The ground-based CRS was assessed for continuous measurements at the low-SWE, Elora site, and high-SWE, TVC site. This allowed both winter seasons to be compared to one another. It is important to note that the CRS-calculated SWE and non-melt (non-zero) snow survey measurement values from the 2016/17 winter season at the Elora site were adjusted to account for the antecedent water storage found in the top few centimeters of soil, as explained in sections *1.8.3* and *2.4.1.* Additionally, please note that the CRS-measured SWE was obtained using equation *2.4.*

2.4.2.1. Continuous measurement of SWE at the low-SWE, Elora site

Due to the CRS's continuous ability to measure SWE, a full winter season dataset can be obtained and compared. Unfortunately, due to setting up the ground-based CRS late in the 2016/17 winter season (February 11), only a partial dataset is available for this year. Using this approach, it is clear that the 2016/17 season had a maximum SWE of only 31 mm while the 2017/18 dataset peaked at 42 mm. Interestingly, both seasons experienced their most prominent decrease in SWE in the immediate day(s) after they reached their peak. Additionally, it is also interesting to note that during the February 11 to February 20 time period, the 2017/18 dataset consistently displayed negative SWE values, while in 2016/17, SWE values were constantly above 10 mm. When the CRS-measured SWE values go below 0 mm, this simply implies that the CRS is sensing a lower SWE than its baseline, meaning that the immediate surrounding environment is drier compared to when the ground-based CRS was first installed. Another comparison can be made in relation to when the site became snow-free in each season. In 2016/17 this was on March 14, while in 2017/18 this occurred over 3 weeks earlier on February 20. Please note that the constant increases and decreases of SWE (Figs. 2.8 and 2.9) is directly due to the change in snow dynamics (sublimation of snow grains, wind erosion/transport), and the inherent measurement error of the CRS's 12-h averaged moderated neutron count (1-12%).

Similar to the 2016/17 winter season, SWE values from the ground-based CRS during the 2017/18 winter season match exceptionally well to values obtained from snow surveys on the same dates (Fig. 2.8b). However, there are a few notable discrepancies which should be addressed. The first instance is found on January 8, 2018, where the CRS recorded a SWE of 9 mm while a snow survey conducted on this day gave a SWE value of 29 mm. We believe this

was attributed to the inherent measurement errors that result from manual snow surveying. A similar incident occurs on February 1, 2018 where the CRS records a SWE reading of 2 mm

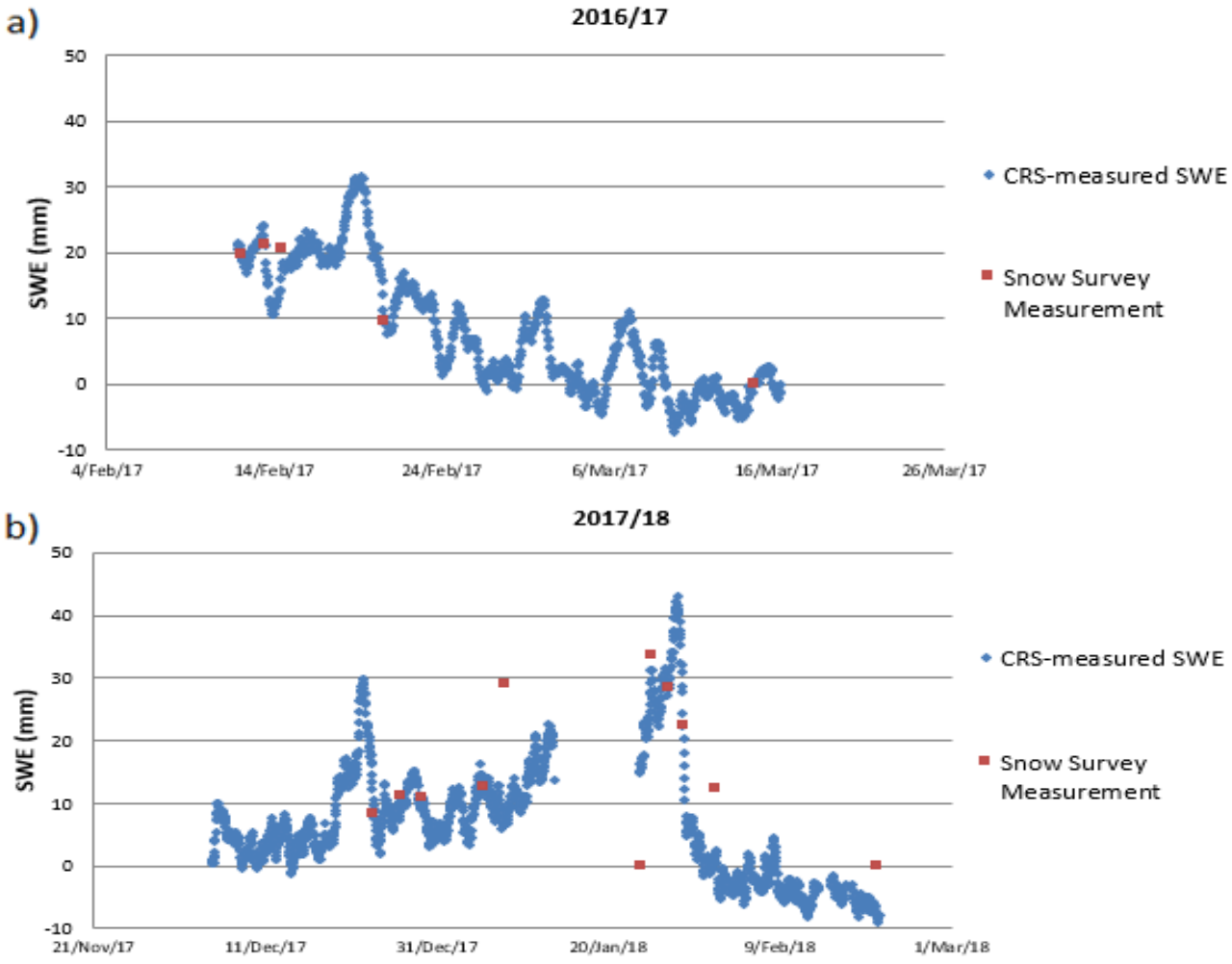

Figure 2.8. Continuous measurement of SWE at the low-SWE, Elora site during the **a)** 2016/17 winter season and **b)** during the 2017/18 winter season.

while a snow survey conducted on the same day indicated 12 mm. Once again, we suspect errors associated with manual snow surveying played a role. The final interesting occurrence from this season occurred on January 23, 2018. During this time the CRS measured a SWE of 16 mm

while a snow survey conducted on the same day resulted in a SWE of 0 mm. This discrepancy occurred because of a warm spell that lead to rapid snowmelt between January 21-22, immediately followed by a return to below freezing temperatures which caused the melted snow water to refreeze and create thick ice layers throughout the site. When a snow survey was conducted on this day, the snow tube was not able to cut through or measure the ice lenses, and no snow was present on the ground, hence the snow survey value being recorded as 0 mm. On the other hand, since the ground-based CRS measurement principle works by an attenuation of neutrons via hydrogen, the CRS appeared to have no issue with measuring the water equivalent in ice. This is a prominent advantage of the ground-based CRS.

2.4.2.2. Continuous measurement of SWE at the high-SWE, TVC site

SWE values measured by the 5 ground-based CRSs were averaged and compared to averaged snow survey data from the same date. As the initial snow-precipitation events of the 2016/17 season occurred (starting in November, 2017), SWE increased to 62 mm (by mid-December, 2017). SWE continues to increase until March, 2017. From March to mid-May, 2017, SWE consistently stays between 330 and 370 mm. This 40 mm variability in SWE is directly related to blowing snow, the sublimation of snow grains, and the inherent margin of error of the CRS's 12-h averaged moderated neutron count (1-12%). Averaged snow survey SWE values at this site show an excellent correlation to the CRS-measured SWE where most manual snow survey measurements generally overlap the CRS-measured SWE and were able to capture the relative minimum and maximum (Fig. 2.9a). It is important to note that during the end of winter melt-period in the 2016/17 season (May 19 to May 31), the CRS appears to underestimate SWE when compared to the averaged snow survey measurements conducted on the same dates (May 28, May 31). We suspect this is directly related to meltwater infiltrating into the soil and leaving

the ground-based CRS's measurement scope. Interestingly, although they used an above-ground sensor, this contrasts findings from Sigouin and Si (2016) who found that their CRS tended to overestimate SWE during melt events.

Similar trends are seen in the 2017/18 dataset (Fig. 2.9b). By incorporating multiple ground-based CRSs in a transect, snowdrifts can be compared from year-to-year. For example, from Figure 2.9 it is evident that snow-precipitation occurred earlier in 2017/18 when compared to the 2016/17 winter season. By mid-November, SWE was noted as 128 mm in 2017/18 while during this time in 2016/17 it was still near 0 mm. Similarly, the snowdrift in both years saw the greatest accumulation of SWE in mid-March. Although the pattern of SWE increase is not similar between the two years, the averaged peak SWE is, in 2017/18 it was 357 mm while in 2016/17 it was 369 mm. Similar to results found in 2016/17, the CRS-measured SWE in 2017/18 underestimated the averaged SWE from snow surveys during the melt phase (June 6, 2018), this is likely due to melt-water infiltrating deep enough into the soil where it exited the ground-based CRS measurement scope. These examples demonstrate some potential capabilities of the ground-based CRS when continuously measuring a specific snow patch in high-SWE environments.

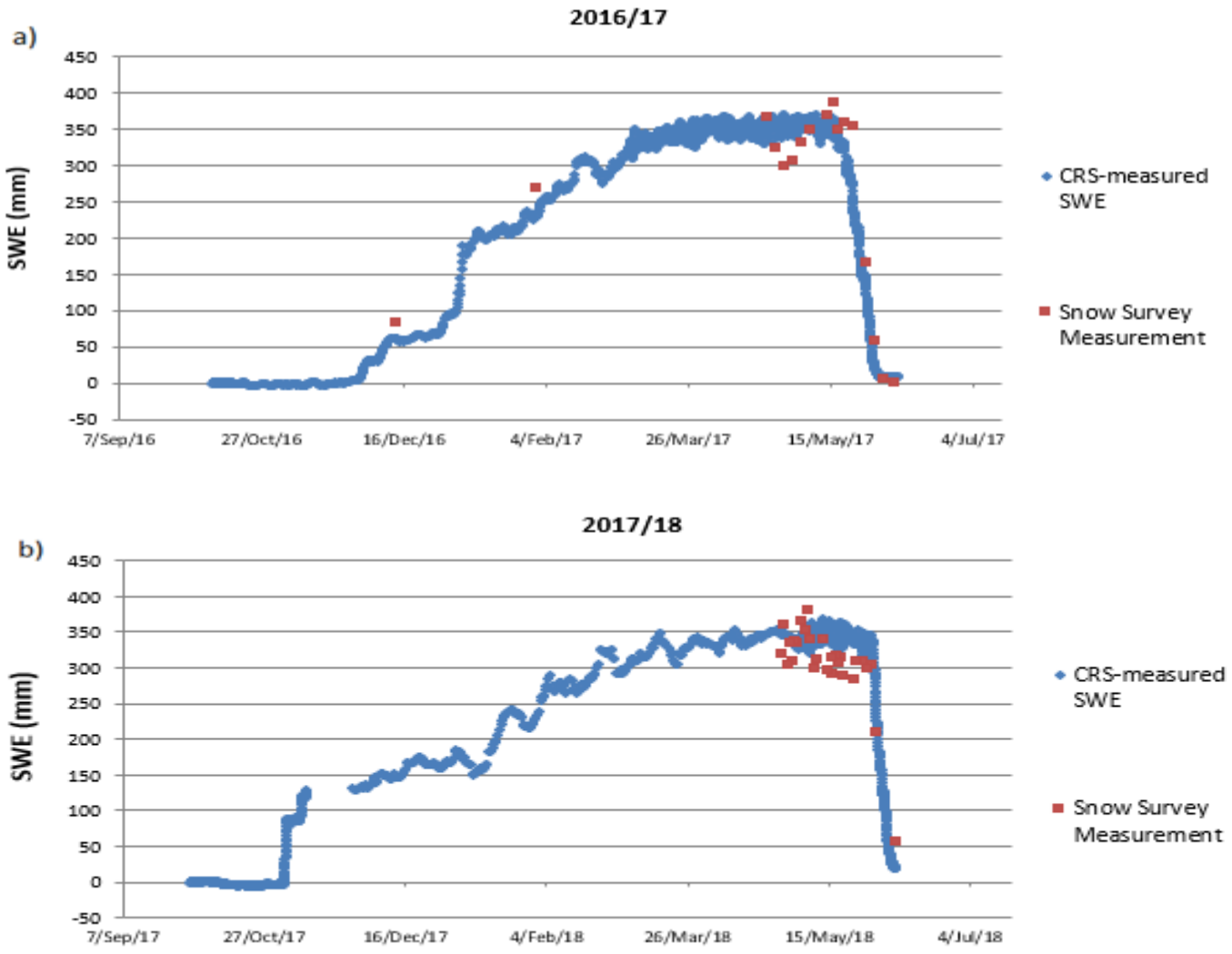

Figure 2.9. Continuous measurement of a snowdrift in the **a)** 2016/17 winter season and **b)** 2017/18 winter season.

2.4.3 Application of the ground-based CRS for an in-depth Assessment of Specific Snowdrifts

The 5 ground-based CRSs from the TVC transect were individually assessed in order to examine the profile of the snowdrift and its change throughout the winter season. Although this transect was only 50 m in length, each CRS experienced a noticeable amount of variability in SWE. The CRS at the margin of this transect (CRS 1) experienced the largest differences relative

to the CRSs in the middle of the transect (CRSs 2-5) which have shrubs up to 1.5 m tall and trap blowing snow. CRS 1 received less snow accumulation than the other CRSs in this transect due to a lack of accumulation from blowing snow because of its position within the site being outside of the shrub patch and instead, within the surrounding tundra landscape. From Figure 2.10ab, it is evident that each CRS noted a sharp increase in SWE in response to the initial snow-precipitation events of the season. As expected, CRS 1 measured the lowest increase in SWE (Fig. 2.10ab). Similarly, CRS 2 measured the second lowest increase in SWE. Contrastingly, due to CRS 4's position being approximately in the middle of the TVC transect where there are tall alder shrubs, this location experiences a larger accumulation of snow, and therefore CRS 4 experienced the largest increase in SWE (Fig. 2.10ab). While mid-season snow-precipitation events decrease the moderated neutron intensity, it is not by the same magnitude as the initial snowfall events of the season. This occurrence can be seen when comparing the change in SWE at the very start of the winter season to the mid- and end-of-winter in both 2016/17 and 2017/18 (Fig. 2.10ab).

An interesting application of the ground-based CRS system can be used when assessing snowdrifts. By setting up the CRS instruments at two linear margins of the snowdrift, as well as additional CRSs within the snowdrift, the melt dynamics can be examined. Unfortunately, due to CRS 6 becoming unresponsive prior to beginning this research, a thorough analysis of this occurrence could not be completed. However, a partial analysis could. By individually assessing each CRS within the transect, we were able to assess how much accumulation occurs within the snowdrift as well as the amount of melt that occurs at the boundaries. For example, from Figure 2.10a, it is clear that CRS 1 experiences melt the earliest in the season, starting at May 16, followed by CRS 5 at May 18, CRS 2 and 3 on May 21 and lastly, May 26 for CRS 4. By June 7,

all 5 CRSs in this transect have melted (0 SWE). By applying the ground-based CRSs using this unique approach, specific snowdrifts or snow covers with prominent significance to their environments can be assessed in detail.

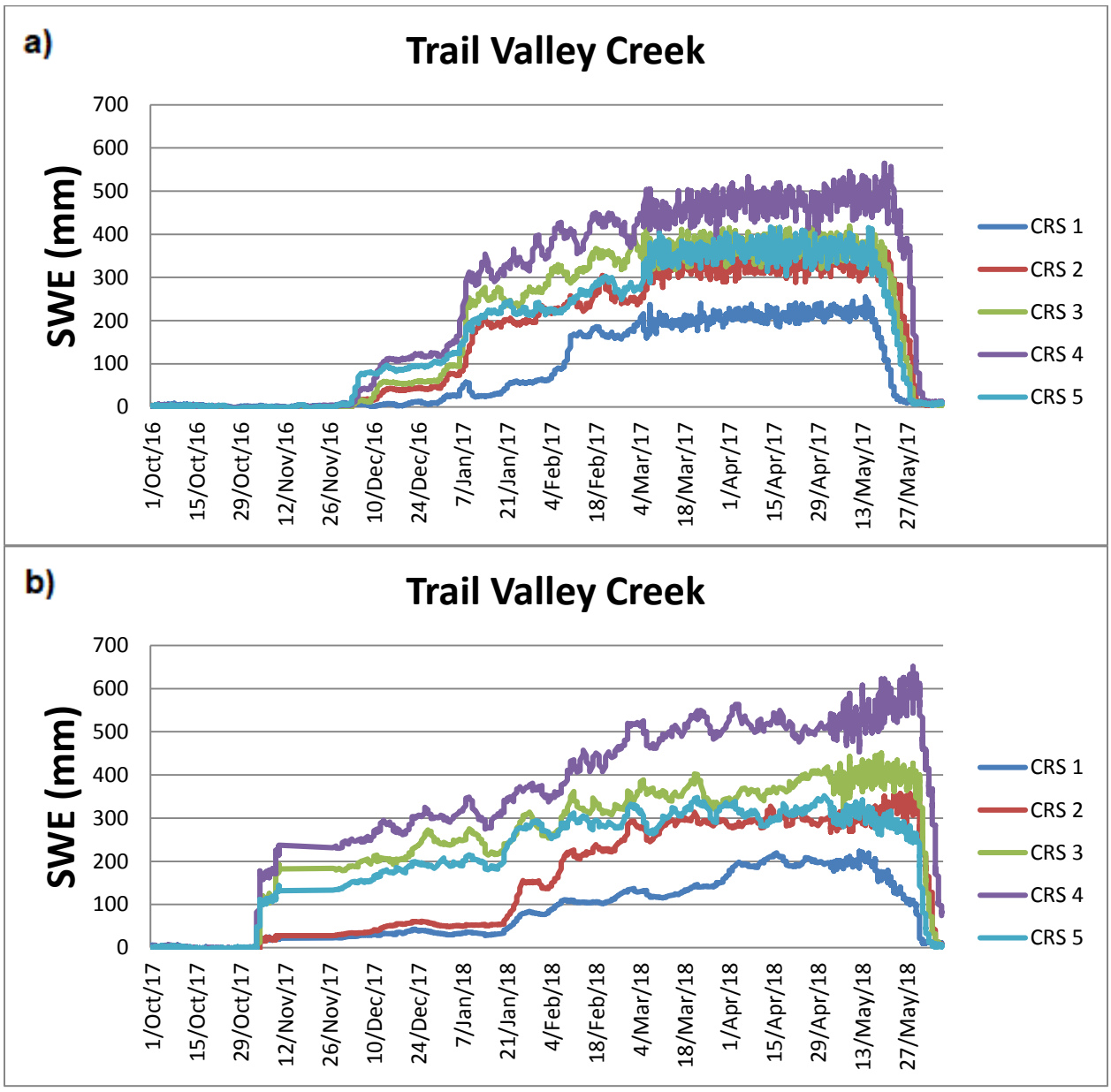

Figure 2.10. Change in SWE from each individual ground-based CRS throughout the winter season. **a)** 2016/17 and **b)** 2017/18 winter season.

Similar trends were noted at the TVC snowdrift between the 2016/17 and the 2017/18 winter seasons (Fig. 2.10ab). When comparing the two datasets, it is clear that the maximum CRS-measured SWE in the 2016/17 winter season was 507 mm, while in 2017/18 it was 620 mm. Both peak values were recorded by CRS 4. Please note that the sudden noisiness of Figure 2.10ab starting in March 4, 2017 in the 2016/17 season and April 30, 2018 in the 2017/18 season is due the change in frequency of the sampling rate. This change in frequency occurred when we switched the CRS system from winter power conservation mode, which had 4, 1-hour interval recordings per day, to summer power conservation mode, which had 24, 1-hour interval recordings per day.

An additional analysis of the snowdrift profile at TVC was conducted by comparing SWE recorded by each CRS and correlating it to its corresponding snow survey measurement within the transect (Fig. 2.11). Three dates were chosen from the 2016/17 season; May 2, 2017, to represent the end of winter snowpack which has not undergone melt, May 28, 2017, to represent the end of winter snowpack which has begun to melt, and June 3, 2017, to represent nearly the complete melt of this snowdrift. From visual inspection, it is clear individual snow survey measurements corresponded exceptionally well to the SWE measured by the CRSs. R^2 values for these dates are 0.91, 0.94 and 0.99 respectively. These high R^2 values support the notion that each CRS has great accuracy in predicting SWE directly overlying it.

By examining individual ground-based CRSs in a transect such as this, the dynamics in SWE can be assessed in considerable detail and a definitive snow-profile can be created. Using Figure 2.11 as an example, as expected, the snowdrift appears in a concave-down parabola-esque shape during pre-melt conditions (Fig. 2.11a). Then, during melt conditions, the snowdrift experiences the largest magnitude of melt at its margins (Fig. 2.11b), before lastly, the body of

the snowdrift melts (Fig. 2.12c). It is important to note that although the CRS transect follows the expected trends, values from CRS 3 and CRS 5 on May 28, were found to underestimate SWE compared to manual snow survey measurements. We believe this is related to meltwater infiltrating the soil and exiting the measurement scope of the CRS instrument, however, when a snow survey was conducted, the soil plug at the base of the snow core sample was supersaturated causing some water to leak into the snow core sample and therefore lead to a larger density measurement which led to a larger SWE calculation. Additionally, through Figure 2.11, it is clear that CRS 1 records the smallest volume of SWE, and that SWE increases until reaching its peak at CRS 4, past this (towards CRS 5), SWE declines. The snow survey results from Figure 2.11 correlate well with the expected trends displayed in Figure 2.10. It is important to note that on June 3, all snow survey SWE values were recorded as 0 mm except CRS 4, which was measured to be 38 mm. However, the CRSs during this time recorded SWE values slightly above 0 mm (7, 6, 6, 35, and 7 mm respectively). This is likely attributed to the CRSs being affected by the soil-saturated meltwater surrounding them and therefore displaying non-zero values even though the snow has almost entirely melted.

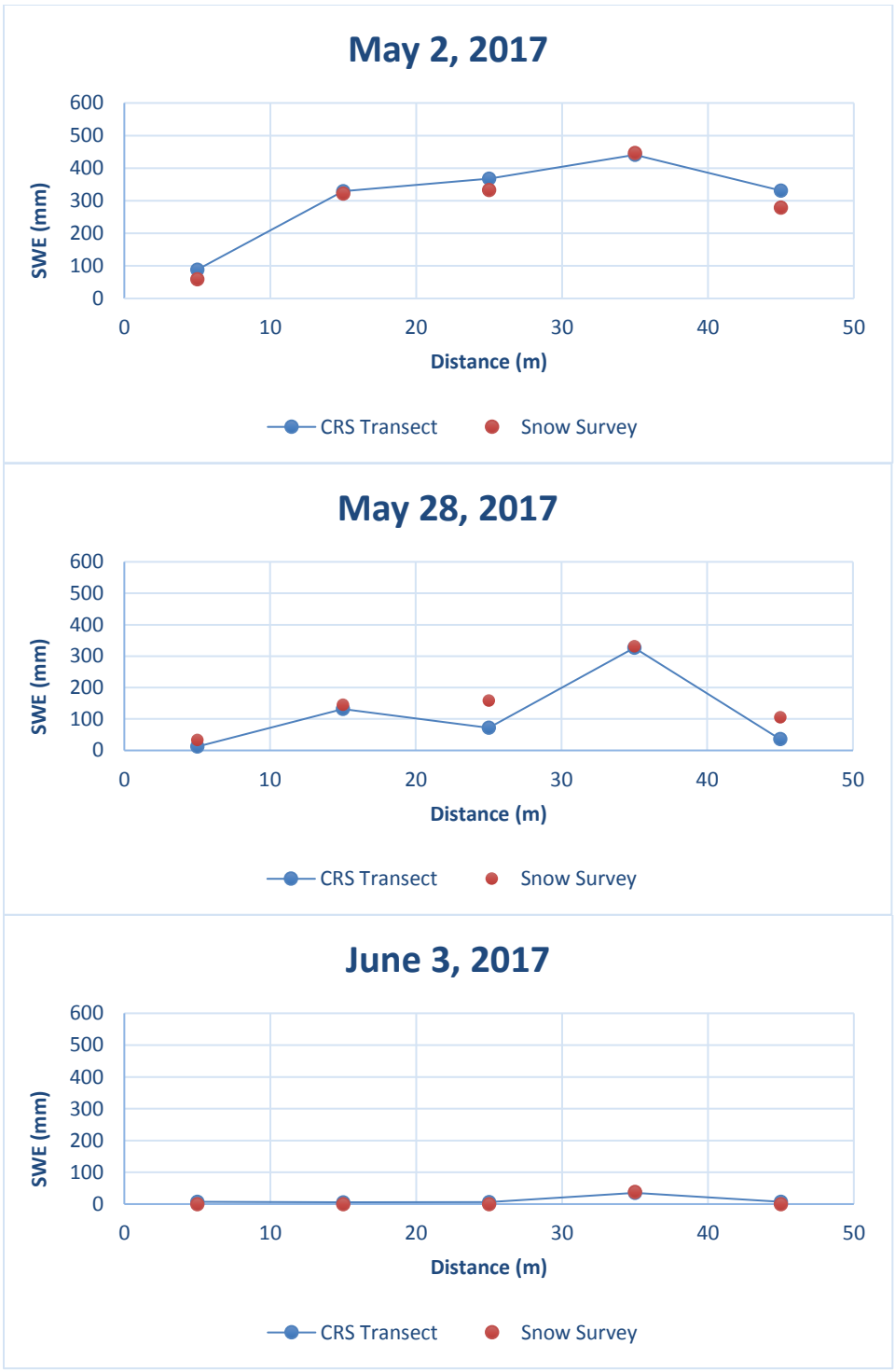

Figure 2.11. Trail Valley Creek snowdrift profile from the 2016/17 winter season. **a)** end of winter snowpack which has not undergone melt, **b)** end of winter snowpack which has begun to melt, and **c)** nearly complete melt of this snowdrift. CRS-1 is located about 5 m from the start of the transect and each following CRS about 10 m further until reaching CRS-5 at 45 m.

2.4.4 Conclusions

The ground-based CRSs were tested at both a low-SWE rural site in Elora, Ontario and high-SWE Arctic site in TVC, Northwest Territories. A strong negative correlation (*r* values between -0.70 and -0.95) was found between the moderated neutron intensity and density/depth for each site and year. Corresponding R^2 values were also found to be relatively strong (0.49 to 0.91), but exhibited some variability year-to-year. Even so, when examining the similarity of trend lines for each year and site, a definitive relationship clearly exists; as depth increases, density increases, and in turn SWE increases as well, subsequently decreasing the neutron intensity. An even stronger negative correlation (*r* values between -0.89 and -0.98) was found between the CRS-measured neutrons and the manual SWE measurements obtained from snow surveying over two winter seasons at both sites. Corresponding R^2 values were found to be extremely strong (0.79 to 0.96), which led to the formation of empirical equations that can, in some instances, be used to predict SWE values at their respective site. Please note that all CRS-measured SWE in this work was obtained using equation *2.4* and were verified via snow surveys. Overall, the CRS system demonstrated that it was able to measure SWE at both sites with an extremely strong accuracy.

There are several unique advantages of using a ground-based CRS to measure SWE:

- The ground-based CRS provides a continuous measurement of SWE throughout the winter season.
- The ground-based CRS can be installed in remote locations and in terrains where snow surveys are difficult to conduct.
- The ground-based CRS replaces the need of manually conducting snow surveys for SWE measurements.

- The ground-based CRS appears to effectively measure the SWE of dry snow, ice layers, and wet snow without bias.

A few limitations arise when using the ground-based CRS to measure SWE:

- In order to establish a baseline SWE value for the winter season, the ground-based CRS should be installed 7-14 days prior to the initial snow-precipitation events of the winter season. Otherwise, the antecedent water content in the top few centimeters of soil must be known and added to the CRS-measured SWE and snow survey values.
- During large magnitude melt events, the ground-based CRS tended to underestimate SWE compared to values obtained from snow surveys. Although they used an above-ground sensor, this contrasts findings from Sigouin and Si (2016) who found that their CRS tended to overestimate SWE during melt events.
- Solar power may not be sufficient to power the CRS system through a harsh Arctic winter, and other sources of energy, such as wind or sufficiently large batteries, may be required.

Future research should determine at what soil depth the ground-based CRS is impacted by soil water content when a snowpack is present, and future studies should reprogram the CRS measurement interval to 15 minutes in order to assess blowing snow events.

3. CONCLUSIONS, FUTURE RESEARCH AND APPLICATIONS

3.1 Summary of Findings and Conclusions

The potential for monitoring SWE with a ground-based CRS was tested in a rural field in southern Canada that is representative of a temperate, low-SWE environment and in a deep snowdrift in the Arctic which is representative of a typical high-SWE environment. A negative correlation was noted between the CRS measured neutrons, density, depth and manual SWE measurements obtained from snow surveying over two winter seasons. Empirical equations (equations 2.7-2.10) were created from the relationship between the neutron intensity and averaged snow survey SWE data and can, in some instances, be used to estimate SWE from the CRS-measured neutrons. Strong Pearson correlation coefficients ranging between -0.89 and -0.98, and R^2 values between 0.79 and 0.96 from both sites and years demonstrate the strong potential of the ground-based CRS system for SWE measurements. Although the CRS experienced some discrepancies in SWE when compared to manual measurements, it was able to accurately capture the relative minimum and maximum SWE at both sites and during both years.

It was found that low-SWE sites using the ground-based CRS require the establishment of a baseline which is acquired by installing the CRS instrument 7-14 days prior to the initial snow-precipitation events of the winter season. Otherwise, the antecedent water content in the top few centimeters of soil should be known and added to the CRS and snow survey SWE values. For high-SWE sites, this soil water storage is negligible (Paquet et al., 2008; Howat et al., 2018). This research showed the potential of the ground-based CRS's ability to provide consistent annual monitoring in regions with seasonal or persistent snow cover. Since data from the CRS can be transmitted in real time via satellite, the use of CRS systems are ideal for remote

locations. A prominent advantage of the CRS was noted when it appeared that the water equivalent from ice layers was accurately recorded by the sensor (Desilets et al., 2010; Siguoin and Si, 2016). The ability of the CRS to measure, dry snow, wet snow, and ice layers, is due to the fact that neutrons are directly attenuated by any hydrogen overlying the sensor. In addition, similar to findings from Desilets et al. (2010), Sigouin and Si (2016), Schattan et al. (2017), and Howat et al. (2018), it was noted that the initial snow-precipitation events of the winter season caused the neutron intensity to decrease by a larger magnitude than snow-precipitation events that occur throughout the winter season. Separately, the CRS recorded a maximum SWE of 620 mm in the 2017/18 winter season, in-line with the manufacturer statement that there is no practical limit to the amount of SWE the sensor can detect, and similar to results found by Howat et al. (2018). This research confirmed that the ground-based CRS can be easily installed in any terrain, and in locations where consistent snow surveys are not practical.

In contrast to results noted by Kodama et al. (1979), we found that when examining the relationship between moderated neutrons counts measured by the CRS and SWE values obtained from snow surveys, an exponential regression performed considerably worse (0.55) when compared to a linear regression (0.89).

It is important to note that all empirical equations created within this work are site-specific. In addition, it is not advised to use the CRS empirical equations formulated in this study as a primary method to predict future SWE. This is because each empirical equation is only directly representative of the seasonal dynamics involved during that specific winter season. Meaning that while the equations do provide insight of predictive potential at these sites, they do not directly incorporate significant variables, such as the barometric pressure or the temporal cosmic ray flux, which have potential to vary considerably over short and/or long timeframes.

The equations are recommended to be used when the user is interested to quickly estimate a reasonable potential amount of SWE at the specific site the CRS was corrected for. The longer duration that the empirical formulas are used in a season, the larger margin of error they output and the more unreliable their results become. An exception to using the empirical formula as a primary method to predict SWE can be made if the CRS instrument has been continuously operating at the same site for multiple winter seasons and the empirical equations from past seasons are averaged to create one equation representative of the specific site. We recommend incorporating a running average of 3 winter seasons. Although this will minimize impacts from individual weather events, it will provide the most probable values of SWE that are to be expected at the site of interest. Both approaches have their own set of advantages and disadvantages and should be incorporated where and when appropriate.

Since the CRS is commonly powered by solar energy, a problem may arise if the battery systems are too small and when there is limited sunlight for extended periods of time. This issue is amplified in the Arctic, where there is perpetual darkness for weeks, preceded and followed by days with faint sunlight, similar to a dusk/dawn setting. To overcome this, we recommend using larger battery systems and incorporating other sources of energy, such as wind, to provide power to the CRS system. Another limitation of the CRS is that during large magnitude melt events, the ground-based CRS tended to underestimate SWE compared to values obtained from snow surveys. We suspect this is due to meltwater infiltrating into the soil and leaving the CRS's measurement scope. Although they used an above-ground CRS, this contrasts findings from Sigouin and Si (2016), who noted that the CRS tended to overestimate SWE during melt events.

Interestingly, although neutron theory related to CRSs suggests that low-SWE sites inherently have considerably larger margins of error for SWE estimations, this research found

that the low-SWE site performed better than the high-SWE site when comparing snow survey measurements to the moderated neutron counts, this is supported by the Pearson correlation coefficients. More studies are needed to confirm this discrepancy.

3.2 Future Research

Since it was found that soil water in the top soil profile directly surrounding the ground-based CRS affected the neutron intensity, future research involving a ground-based CRS at a low-SWE site should determine at what soil depth the ground-based CRS is impacted by soil water content. Although this research tested the CRS at a low- and high-SWE environment, it is recommended that future studies assess the CRS using additional low- and high-SWE sites. Future research should incorporate the ground-based CRS along a steep slope margin such as a ridge or mountain overhang in order to assess snow accumulation across transects with even larger variability in snow depth. In addition, ground-based CRS transects should be set up in sites where they are able to assess, in detail, the impact of short, moderate, and tall vegetation on snow accumulation and melt. Since it appeared that ice layers are measured by the ground-based CRS without bias, additional research related to this topic should be explored. Future research should reprogram the CRS measurement interval to 15 minutes (from 1-h) to be able to provide a more detailed analysis of snow dynamics, especially in relation to small, moderate, or large snow-precipitation and blowing snow events. Lastly, future research should include precipitation data to support neutron intensity increases and decreases.

This work demonstrated that CRSs installed in the Arctic have potential for providing real time observations of changes in SWE at remote, unmanned, sites. We recommend that CRS systems be installed along prominent snow drift areas to estimate the SWE potential during the end of winter/start of spring melt. Additionally, similar to the CRS network that Électricité de

France operates, this idea can be expanded into a network of CRS that would be installed near rivers and would provide observational data related to hydro-electric energy. This would be especially beneficial in the Northwest Territories since 75% of the electricity is from hydro sources (NTPC, 2013). Lastly, by installing CRS systems in troublesome terrains, such as ridges or mountain overhangs, unique datasets can be obtained and used for developing snow models which can aid in water resource management as well as avalanche and flood forecasting.

APPENDICES

APPENDIX A. ADDITIONAL FIGURES

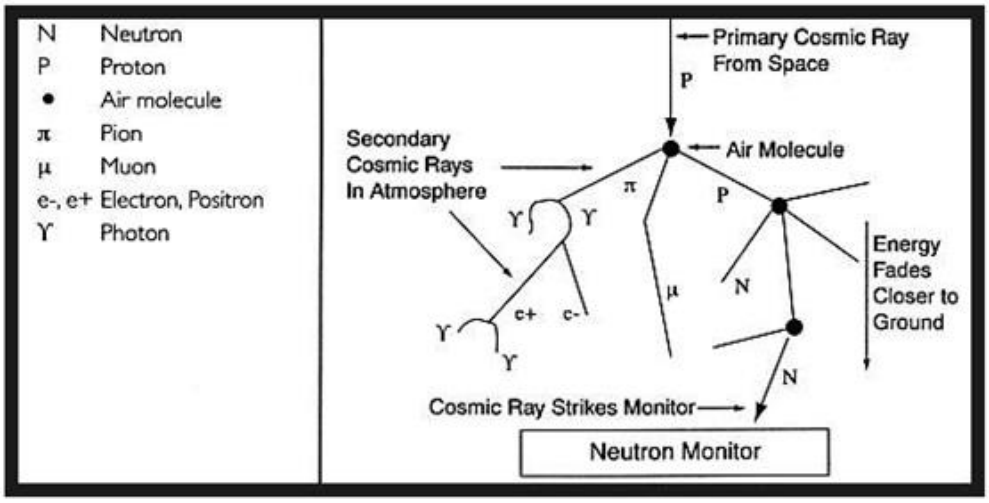

Figure A.1. Movement of cosmic rays in the atmosphere. Primary cosmic rays enter the atmosphere and impact with a molecule. This collision produces a cascade of new secondary cosmic ray particles. Each secondary cosmic ray carries with it a part of the energy and continues colliding with other atmospheric molecules as it moves closer towards Earth's surface. Neutrons are the secondary-cosmic ray of focus in this research. Figure and caption are from Bartol (1999).

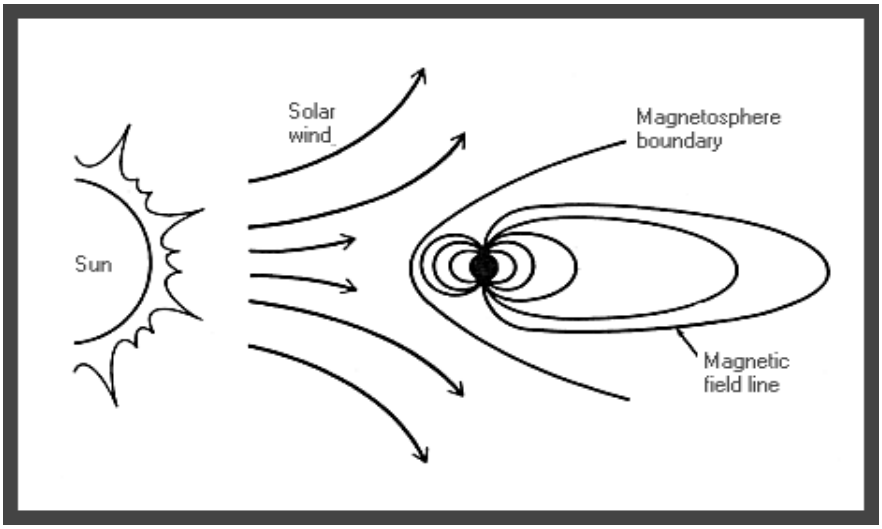

Figure A.2. Cosmic rays will encounter Earth's magnetic field and be guided along the field lines towards the Polar Regions. Figure is from Bartol (1999).

APPENDIX B. DATA

Table B.1. Averaged snow survey data for the Elora site in 2016/17. Values are rounded.

Elora – 2016/17			
Date	**SWE (mm)**	**Depth (cm)**	**Density (kg/m^3)**
11-Feb	14	7	216
13-Feb	18	15	112
14-Feb	15	7	228
20-Feb	6	5	117
14-Mar	0	0	0

Table B.2. Averaged snow survey data for the Elora site in 2017/18. Values are rounded. Data from January 16 and 19 was excluded due to the CRS not recording during these times.

Elora - 2017/18			
Date	**SWE (mm)**	**Depth (cm)**	**Density (kg/m^3)**
23-Dec	4	6	74
27-Dec	11	10	107
30-Dec	11	11	98
05-Jan	11	10	111
08-Jan	29	16	184
23-Jan	0	0	0
25-Jan	34	22	151
27-Jan	28	17	167
28-Jan	24	7	332
01-Feb	12	9	139
20-Feb	0	0	0
16-Jan	2	4	59
19-Jan	5	4	121

Table B.3. Averaged snow survey data for the Trail Valley Creek shrub patch transect in 2016/17. Values are rounded.

Trail Valley Creek - 2017/18			
Date	**SWE (mm)**	**Depth (cm)**	**Density (kg/m^3)**
13-Dec	82	44	178
01-Feb	268	86	294
23-Apr	364	115	323
26-Apr	322	101	302
29-Apr	297	98	284
02-May	304	64	301
05-May	331	104	301
08-May	346	100	335
14-May	367	106	333
16-May	385	100	376
18-May	347	84	378
20-May	358	83	387
21-May	351	87	429
28-May	164	35	406
31-May	57	13	252
03-Jun	4	2	71
06-Jun	0	0	0

Table B.4. Averaged snow survey data for the Trail Valley Creek shrub patch transect in 2017/18. Values are rounded.

Trail Valley Creek - 2017/18			
Date	**SWE (mm)**	**Depth (cm)**	**Density (kg/m^3)**
28-Apr	318	98	300
29-Apr	362	107	331
30-Apr	302	93	311
01-May	333	100	317
02-May	308	96	309
03-May	336	101	321
04-May	334	102	314
05-May	364	105	334
06-May	350	104	312
07-May	380	111	343
08-May	338	107	311
10-May	294	89	318
11-May	312	91	334
13-May	339	98	339
14-May	296	91	308
15-May	284	88	320
16-May	312	84	342
17-May	315	88	325
18-May	304	81	338
19-May	315	87	330
20-May	287	81	314
23-May	284	81	314
24-May	310	79	346
27-May	307	82	335
28-May	299	76	360
29-May	303	79	352
31-May	209	67	293
07-Jun	55	17	164

Table B.5. 2016/17 Elora regression analysis summary statistics between averaged snow survey SWE and CRS-measured moderated neutron counts averaged over 12-h.

Regression Statistics	
Multiple R	0.958981
R Square	0.919645
Adjusted R Square	0.89286
Standard Error	2.409218
Observations	5

ANOVA

	df	*SS*	*MS*	*F*	*Significance F*
Regression	1	199.287	199.287	34.3342	0.009911
Residual	3	17.41299	5.80433		
Total	4	216.7			

	Coefficients	*Standard Error*	*t Stat*	*P-value*	*Lower 95%*	*Upper 95%*	*Lower 95.0%*	*Upper 95.0%*
Intercept	112.0306	17.429	6.427826	0.007633	56.56372	167.4974	56.56372	167.4974
X Variable 1	-0.08439	0.014403	-5.85954	0.009911	-0.13023	-0.03856	-0.13023	-0.03856

Table B.6. 2016/17 Elora regression analysis summary statistics between averaged snow survey SWE and CRS-measured moderated neutron counts averaged over 12-h. Values are adjusted to account for antecedent soil water storage.

Regression Statistics	
Multiple R	0.978353
R Square	0.957175
Adjusted R Square	0.9429
Standard Error	2.19561
Observations	5

ANOVA

	df	*SS*	*MS*	*F*	*Significance F*
Regression	1	323.2379	323.2379	67.05202	0.003811
Residual	3	14.46211	4.820703		
Total	4	337.7			

	Coefficients	*Standard Error*	*t Stat*	*P-value*	*Lower 95%*	*Upper 95%*	*Lower 95.0%*	*Upper 95.0%*
Intercept	143.9154	15.8837	9.060571	0.00284	93.36635	194.4644	93.36635	194.4644
X Variable 1	-0.10748	0.013126	-8.18853	0.003811	-0.14925	-0.06571	-0.14925	-0.06571

Table B.7. 2017/18 Elora regression analysis summary statistics between averaged snow survey SWE and CRS-measured moderated neutron counts averaged over 12-h.

Regression Statistics	
Multiple R	0.968442
R Square	0.937879
Adjusted R Square	0.930977
Standard Error	3.016122
Observations	11

ANOVA

	df	*SS*	*MS*	*F*	*Significance F*
Regression	1	1236.087	1236.087	135.8787	9.86E-07
Residual	9	81.87291	9.09699		
Total	10	1317.96			

	Coefficients	*Standard Error*	*t Stat*	*P-value*	*Lower 95%*	*Upper 95%*	*Lower 95.0%*	*Upper 95.0%*
Intercept	191.9347	15.18032	12.64365	4.93E-07	157.5944	226.2749	157.5944	226.2749
X Variable 1	-0.14382	0.012338	-11.6567	9.86E-07	-0.17173	-0.11591	-0.17173	-0.11591

Table B.8. Original combined data for the 2016/17 & 2017/18 Elora regression analysis summary statistics between averaged snow survey SWE and CRS-measured moderated neutron counts averaged over 12-h.

Regression Statistics	
Multiple R	0.882606
R Square	0.778993
Adjusted R Square	0.764259
Standard Error	5.15501
Observations	16

ANOVA

	df	*SS*	*MS*	*F*	*Significance F*
Regression	1	1405.003	1405.003	52.87109	2.73E-06
Residual	14	398.612	26.57413		
Total	15	1803.615			

	Coefficients	*Standard Error*	*t Stat*	*P-value*	*Lower 95%*	*Upper 95%*	*Lower 95.0%*	*Upper 95.0%*
Intercept	163.1945	20.7115	7.879413	1.04E-06	119.049	207.34	119.049	207.34
X Variable 1	-0.12264	0.016866	-7.27125	2.73E-06	-0.15859	-0.08669	-0.15859	-0.08669

Table B.9. Combined 2016/17 & 2017/18 Elora regression analysis summary statistics between averaged snow survey SWE and CRS-measured moderated neutron counts averaged over 12-h. 2016/17 values are adjusted to account for antecedent soil water storage.

Regression Statistics	
Multiple R	0.942792
R Square	0.888856
Adjusted R Square	0.881446
Standard Error	3.722622
Observations	16

ANOVA

	df	*SS*	*MS*	*F*	*Significance F*
Regression	1	1662.394	1662.394	119.9598	1.49E-08
Residual	14	207.8688	13.85792		
Total	15	1870.262			

	Coefficients	*Standard Error*	*t Stat*	*P-value*	*Lower 95%*	*Upper 95%*	*Lower 95.0%*	*Upper 95.0%*
Intercept	177.5616	14.95654	11.87184	5.01E-09	145.6825	209.4407	145.6825	209.4407
X Variable 1	-0.1334	0.01218	-10.9526	1.49E-08	-0.15936	-0.10744	-0.15936	-0.10744

Table B.10. 2016/17 Trail Valley Creek regression analysis summary statistics between averaged snow survey SWE and CRS-measured moderated neutron counts averaged over 12-h.

Regression Statistics	
Multiple R	0.952625
R Square	0.907494
Adjusted R Square	0.901327
Standard Error	42.82677
Observations	17

ANOVA

	df	*SS*	*MS*	*F*	*Significance F*
Regression	1	269896	269896	147.1519	3.73E-09
Residual	15	27511.98	1834.132		
Total	16	297407.9			

	Coefficients	*Standard Error*	*t Stat*	*P-value*	*Lower 95%*	*Upper 95%*	*Lower 95.0%*	*Upper 95.0%*
Intercept	515.1081	23.76108	21.67865	9.78E-13	464.4626	565.7537	464.4626	565.7537
X Variable 1	-0.6798	0.05604	-12.1306	3.73E-09	-0.79925	-0.56036	-0.79925	-0.56036

Table B.11. 2017/18 Trail Valley Creek site regression analysis summary statistics between averaged snow survey SWE and CRS-measured moderated neutron counts averaged over 12-h.

Regression Statistics	
Multiple R	0.886773
R Square	0.786367
Adjusted R Square	0.77815
Standard Error	27.64541
Observations	28

ANOVA

	df	*SS*	*MS*	*F*	*Significance F*
Regression	1	73143.47	73143.47	95.7039	3.34E-10
Residual	26	19870.98	764.2684		
Total	27	93014.45			

	Coefficients	*Standard Error*	*t Stat*	*P-value*	*Lower 95%*	*Upper 95%*	*Lower 95.0%*	*Upper 95.0%*
Intercept	500.9624	20.63707	24.27488	2.17E-19	458.5423	543.3825	458.5423	543.3825
X Variable 1	-0.71529	0.073117	-9.78284	3.34E-10	-0.86558	-0.565	-0.86558	-0.565

Table B.12. Combined 2016/17 and 2017/18 Trail Valley Creek site regression analysis summary statistics between averaged snow survey SWE and CRS-measured moderated neutron counts averaged over 12-h.

Regression Statistics	
Multiple R	0.934243
R Square	0.87281
Adjusted R Square	0.869852
Standard Error	35.10505
Observations	45

ANOVA

	df	*SS*	*MS*	*F*	*Significance F*
Regression	1	363642.3	363642.3	295.077	7.19E-21
Residual	43	52991.67	1232.364		
Total	44	416634			

	Coefficients	*Standard Error*	*t Stat*	*P-value*	*Lower 95%*	*Upper 95%*	*Lower 95.0%*	*Upper 95.0%*
Intercept	492.0767	13.04336	37.72622	1.36E-34	465.7722	518.3811	465.7722	518.3811
X Variable 1	-0.65368	0.038054	-17.1778	7.19E-21	-0.73043	-0.57694	-0.73043	-0.57694

Table B.13. Final simple regression equations, Pearson correlation coefficients (*r)* and R^2 values for each site and its corresponding year. Note*: $SWE_{Elora2016/17adjusted}$ & $SWE_{EloraCombined}$ incorporated the adjusted SWE values which accounted for the antecedent water storage in the top few cm of soil.

	2016/17	2017/18	Combined
Elora	$SWE_{Elora2016/17adjusted} = -0.107(N_{COR}) + 143.9$ ***r*= -0.98** **R^2= 0.96**	$SWE_{Elora2017/18} = -0.144(N_{COR}) + 191.9$ ***r*= -0.97** **R^2= 0.94**	$SWE_{EloraCombined} = -0.137(N_{COR}) + 177.5$ ***r*= -0.95** **R^2= 0.89**
TVC	$SWE_{TVC2016/17} = -0.679(N_{COR}) + 515.1$ ***r*= -0.95** **R^2= 0.91**	$SWE_{TVC2017/18} = -0.715(N_{COR}) + 500.9$ ***r*= -0.89** **R^2= 0.79**	$SWE_{TVCCombined} = -0.654(N_{COR}) + 492.0$ ***r*= -0.95** **R^2= 0.87**

REFERENCES

Abudu S., Cui C., Saydi M., and King J. (2012) Application of snowmelt runoff model (SRM) in mountainous watersheds: A review. Water Science and Engineering, 5(2), 123-136.

ACIA. (2005) Impacts of a warming Arctic: Arctic climate impact assessment. Cambridge, UK: Cambridge University Press.

Barnett P., Pierce D., Hidalgo H., Bonfils C., Santer B., Das T., Bala G., Wood A., Nozawa T., Mirin A., Cayan D., and Dettinger M. (2008) Human-induced changes in the hydrology of the western United States. Science, 319(5866), 1080-1083.

Bartol J. (1999) Listening for cosmic rays. Based upon report number 5 of the scientific report series of the Aurora Research Institute. Copyright Aurora College, 1999.

Beaumont R. (1965) Mt. Hood pressure pillow snow gauge, J. Appl. Meteorol., 4, 626-631. doi:10.1175/1520-0450(1965)0042.0.CO;2.

Beaumont R. (1967) Field accuracy of volumetric snow samplers at Mt. Hood, Oregon. Physics of Snow and Ice 1, 1007-1013.

Bindon H. (1964) The design of snow samplers for Canadian snow surveys. In Proceedings of the 21st Annual Meeting of the Eastern Snow Conference, Utica, New York, 23-28.

Ball J. (2001) Soil and water relationships. Noble Research Institute. Obtained online from: https://www.noble.org/news/publications/ag-news-and-views/2001/september/soil-and-water-relationships/

Blencowe J. (1960) Soil. Department of Agriculture Bulletin, 462.

Both C., and Visser M. (2001) Adjustment to climate change is constrained by arrival date in a long-distance migrant bird. Nature, 411, 296-298.

Boyd W., Schriever W., and Taylor D. (1981) Snow and buildings. Handbook of Snow: Principles, processes, management and use. Pergamon Press, Toronto, Canada, 562-579.

Buska J., and Tobiasson W. (2001) Minimizing the adverse effects of snow and ice on roofs. Conference on Building Envelope Systems and Technologies. ICBEST-2001. Ottawa, Canada.

Carlson P. (2012) A century of cosmic rays. Phys. Today, 65, 30-36.

Carroll R., and Vadnais G.(1980) Operational airborne measurement of snow water equivalent using natural terrestrial gamma radiation. Proc. 48th Annu. Western Snow Conf., Laramie, WY, Western Snow Conference, pp. 97-106.

Chrisman B., and Zreda M. (2013) Quantifying mesoscale soil moisture with the cosmic-ray rover. Hydrol. Earth Syst. Sci., 17, 5097-5108.

Church E. (1933) Snow surveying: its principles and possibilities. Geogra. Rev., 23(4), 529-563. doi:10.2307/209242.

Coopersmith E., Cosh M., and Daughtry C. (2014) Field-scale moisture estimates using COSMOS sensors: A validation study with temporary networks and leaf-area-indices. J. Hydrol., 519, 637-643.

Clyde D. (1932) Circular 99 – Utah snow sampler and scales for measuring water content of snow. Utah State Agricultural College, Utah Agricultural Experiment Station: Logan, Utah.

CNNRO. (2016) Canadian high arctic research station. Retrieved from http://cnnro.ca/canadian-high-arctic-research-station/.

Crane R., and Anderson M. (1984) Satellite discrimination of snow/cloud surfaces. Int. J. Remote Sensing, 5, 213-223.

Crick P., Dudley C., Glue E., and Thompson L. (1997) Birds are laying eggs earlier. Nature, 411, 296-298.

Crook A., and Freeman T. (1973) A comparison of techniques of sampling the arctic-subarctic snowpack in Alaska. Paper presented at 41st Western Snow Conference, pp 62-68.

Davis R. (1973) Operational snow sensors. Paper presented at 30th Eastern Snow Conference, pp. 57-70.

DeBeer M., and Pomeroy J. (2010) Simulation of the snowmelt runoff contributing area in a small alpine basin. Hydrol. Earth Syst. Sci., 14(7), 1205-1219. doi: 10.5194/hess-14-1205-2010.

Deems J., Painter T., and Finnegan D. (2013) Lidar measurement of snow depth: a review. Journal of Glaciology, 59, 215. doi: 10.3189/2013JoG12J154

Delunel R., Bourles D., van der Beek P., Schlunegger F., Leya I., Masarik J., and Paquet E. (2014) Snow shielding factors for cosmogenic nuclide dating inferred from long-term neutron detector monitoring. Quaternary Geochronology, 24, 16-24.

Derksen C. (2008) The contribution of AMSR-E 18.7 and 10.7 GHz measurements to improved boreal forest snow water equivalent retrievals. Remote Sensing of the Environment, 112(5), 2701-2710.

Derksen C., and Brown R (2012) Spring snow cover extent reductions in the 2008-2012 period exceeding climate model projections. Geophys. Res. Lett., 39, L19504.

Desilets D., and Zreda M. (2003) Spatial and temporal distribution of secondary cosmic-ray nucleon intensities and applications to in-situ cosmogenic dating. Earth and Planetary Science Letters, 206, 21-42. doi: 10.1016/S0012-821X(02)01088-9.

Desilets D., Zreda M., and Ferré A. (2010) Nature's neutron probe: Land surface hydrology at an elusive scale with cosmic rays, Water Resour. Res.46, W11505. doi:10.1029/2009WR008726.

Desilets D., and Zreda M. (2013) Footprint diameter for a cosmic-ray soil moisture probe: Theory and Monte Carlo simulations. Water Resour. Res., 49, 3566-3575. doi:10.1002/wrcr.20187.

Desilets D. (2017) Calibrating a non-invasive cosmic ray soil moisture probe for snow water equivalent. Hydroinnova Technical Document, 17-01, 1.

Dietz J., Kuenzer C., Gessner U., and Dech S. (2012) Remote sensing of snow - a review of available methods. Int. J. Remote Sens., 33(13), 4094-4134.

Dixon D., and Boon S. (2012) Comparison of the SnowHydro snow sampler with existing snow tube designs. Hydrol. Process., 26, 2555-2562.

Dozier J. (1984) Snow reflectance from Landsat-4 thematic mapper. IEEE Trans. Geosci. Remote Sensing GE-22, 323-328.

Dyurgerov M., Bring A., and Destouni G. (2010) Integrated assessment of changes in freshwater inflow to the Arctic Ocean. Journal of Geophysical Research, 115: D12116.

Engman, T., and Gurney J. (1991) Remote Sensing in hydrology. Chapman and Hall, London.

Fang X., and Pomeroy J. (2008) Drought impacts on Canadian prairie wetland snow hydrology. Hydrol. Process. 22(15), 2858-2873.

Farnes E., Peterson R., Goodison E., and Richards P. (1982) Metrication of manual snow sampling equipment. In Proceedings of the 50th Annual Meeting of the Western Snow Conference, Reno, Nevada, 120-132.

FEMA. (2013) Snow load safety guide. Risk management series, FEMA P-957.

Fierz C., Armstrong R., Durand Y., Etchevers P., Greene E., McClung D., Nishimura K., Satyawali P., and Sokratov A. (1999) International classification for seasonal snow on the ground. IHP-VII technical documents in hydrology N∘83, IACS Contribution N∘1, UNESCO-IHP, Paris, UNESCO, Paris.

Foster L., Hall K., and Chang C. (1987) Remote sensing of snow. Eos 68(32), 681-684.

Freeman G. (1965) Snow survey samplers and their accuracy. In Proceedings of the 22nd Annual Meeting of the Eastern Snow Conference, Hanover, New Hampshire, 1-10.

Glynn E., Carroll R., Holman B., and Grasty L. (1988) An airborne gamma ray snow survey of a forest covered area with a deep snowpack. Remote Sensing Environ., 26, 149-160.

Goodison B. (1978) Accuracy of snow samplers for measuring shallow snowpacks: an update. In Proceedings of the 35th Annual Meeting of the Eastern Snow Conference, Hanover New Hampshire, 36-49.

Goodison B., Ferguson H., and McKay G. (1981) Measurement and data analysis, in handbook of snow: principles, processes, management, and use. Pergamon press Canada, Toronto, Canada, pp. 191-274.

Goodison B., Glynn J., Harvey K., and Slater J. (1987) Snow surveying in Canada: A perspective. Can Water Resour. J., 12(2), 27-42.

Goodsite M., Bertelsen R., Pertoldi-Bianchi S., Ren J., Watt L., and Johannsson H. (2016) The role of science diplomacy: a historical development and international legal framework of arctic research stations under conditions of climate change, post-cold war geopolitics and globalization/power transition. Journal of Environmental Studies and Sciences, 6(4), 645-661.

Gray D., Pomeroy J., and Granger R. (1989) Modelling snow transport, snowmelt and meltwater infiltration in open, northern regions. Division of Hydrology, University of Saskatchewan, Saskatoon, Saskatchewan, Canada.

Gray D., Erickson D., and Abbey F. (1974) Energy studies in an arctic environment. Report No. 74-18, Environmental Social Committee, Northern Pipelines Task Force on Northern Oil Development, Information Canada, No. R57- 10/1974, Ottawa, ON. Pp 60.

Hall, K., and Martinec J. (1985) Remote sensing of ice and snow, Chapman and Hall, London.

Hallikainen M., and Jolma P. (1986) Development of algorithms to retrieve the water equivalent of snow cover from satellite microwave radiometer data. In: Proc 1986 International Geoscience and Remote Sensing Symposium (IGARSS 86), Zurich, Switzerland. pp. 611-616.

Harshburger B., Blandford T., Humes K., Walden V., and Moore B. (2005) Evaluation of enhancements to the snowmelt runoff model. Proc. Western Snow Conf. 2005, 57-63.

Hess N., Patterson W., and Wallace R. (1959) Cosmic-ray neutron energy spectrum. Phys. Rev., 116, 445-457.

HESS Collaboration. (2016) Acceleration of petaelectronvolt protons in the Galactic Centre. Nature, 531, 476-479.doi:10.1038/nature17147. PMID 26982725.

Hori M., Sugiura K., Kobayashi K., Aoki T., Tanikawa T., Kuchiki K., Niwano M., and Enomoto H. (2017) A 38-years (1978-2015) northern hemisphere daily snow cover extent product derived using consistent objective criteria from satellite-borne optical sensors. Remote Sensing Environ., 191, 402-418.

Howat I., Peña S., Desilets D., and Womack G. (2018) Autonomous ice sheet surface mass balance measurements from cosmic rays. Cryosphere, 12, 2099-2108. doi: https://doi.org/10.5194/tc-12-2099-2018

IPCC. (2013) Climate change 2013: the physical science basis. Contribution of working group I to the fifth assessment report of the intergovernmental panel on climate change. Cambridge University Press, Cambridge, United Kingdom and New York, NY, USA.

Jenni L., and Kery M. (2003) Timing of autumn bird migration under climate change: advances in long-distance migrants, delays in short-distance migrants. Proc. R. Acad. Sci. B., 270, 1467-1471.

Johnson B. (2004) A theory of pressure sensor performance in snow. Hydrol. Process., 18(1), 53-64. doi:10.1002/hyp.1310.

Johnson B., and Marks D. (2004) The detection and correction of snow water equivalent pressure sensor errors. Hydrol. Process., 18(18), 3513-3525. doi:10.1002/hyp.5795.

Joseph A. (2004) Nuclear Technology. Greenwood Press. Pp. 121-124. ISBN 1-57356-336-6.

Kinar N., and Pomeroy J. (2007) Determining snow water equivalent by acoustic sounding. Hydrol. Process., 21, 2623-2640. doi: 10.1002/hyp.6793.

Kinar N., and Pomeroy J. (2015) Measurement of the physical properties of the snowpack. Rev. Geophys., 53. doi:10.1002/2015RG000481.

Kodama M., Nakai K., Kawasaki S., and Wada M. (1979) An application of cosmic-ray neutron measurements to the determination of the snow-water equivalent. J. Hydrol., 41, 85-92.

Kodama M., Kudo S., Kosuge T. (1985) Application of atmospheric neutrons to soil moisture measurement. Soil Science, 140(4), 237-242.

Köhli M., Schron M., Zreda M., Scmidt U. Dietrich P., and Zacharias S. (2015) Footprint characteristics revised for field-scale soil moisture monitoring with cosmic-ray neutrons. J. Hydrol., 6(4), 1-19.

Krajči P., Kirnbauer R., Parajka J., Schöber J., Blöschl G. (2017) The Kühtai data set: 25 years of lysimetric, snow pillow, and meteorological measurements. Water Resources Research, 53(6), 5158-5165.

Kunzi K., Patil S., and Rott H. (1982) Snow-covered parameters retrieved from NIMBUS-7 SMMR data. IEEE Trans. Geosci. Remote Sensing GE-20, 452-467.

Lange M. (2008) Assessing climate change impacts in the European north. Climatic Change, 87, 7-34.

Lawrence M., and Slater G. (2005) A projection of severe near-surface permafrost degradation during the 21st century. Geophysical Research, 106, 3321-3334.

Liebezeit J., Gurney K., Budde., Zack S., and Ward D. (2014) Phenological advancement in arctic bird species: relative importance of snow melt and ecological factors. Polar Biology, 37(9), 1309-1320.doi:10.1007/s00300-014-1522-x.

Liston G., Perham C., Shideler R., and Cheuvront A. (2016) Modeling snowdrift habitat for polar bear dens. Ecological modelling, 320, 114-134. doi: 10.1016/j.ecolmodel.2015.09.010

Mair M., and Baumgartner D. (2010) Operational experience with automatic snow depth sensors - ultrasonic and laser principle. Central Institute for Meteorology and Geodynamics, Hohe Warte, 38, 1190.

Manabe S., Stouffer J., Spellman J., and Bryan K. (1991) Transient response of a coupled ocean-atmosphere model to gradual changes of atmospheric carbon dioxide. Journal of Climate 7, 5-23.

Marsh P., and Woo M. (1981) Snowmelt, glacier melt, and high arctic streamflow regimes. Can. J. Earth Sci., 18, 1380-1384.

McKay A., and Gray D. (1981) The distribution of snowcover. Handbook of Snow: Principles, Processes, Management and Use. Pergamon Press, Toronto, Canada, 153-190.

Molnau M. (1971) Comparison of runoff from a catchment snow pillow and a small forested watershed. Proc. Western Snow Conf., 39, 39-43.

Moseley T., & Zabierek G. (2006) Guidance on the safe use of lasers in education and research. Electromagnetic radiation at wavelengths extending from 100 nm in the ultra-violet, through the visible (400-700 nm), and the near infrared (700-1400 nm), to the far infrared

(1400 nm – 1 mm). AURPO Guidance Note No. 7. University of Sheffield & University of Birmingham.

Morison J., Aagaard K., and Steele M. (2000) Recent environmental changes in the Arctic: a review. Arctic 53(4), 359-371.

National Snow & Ice Data Center. (2017) Snow Science. University of Colorado.

National Weather Service. (2017) National operational hydrological remote sensing center. Office of water prediction. Chanhassen, MN.

Nester T., Kirnbauer R., Parajka J., and Bloschl G. (2012) Evaluating the snow component of a flood forecasting model. Hydrol. Res., 43(6), 762-779.

Nicholson K., Arthur S., Horne J., Garton E., and DelVecchio P. (2016) Modeling caribou movements: seasonal ranges and migration routes of the central Arctic herd. PLoS ONE 11(4), e0150333. https://doi.org/10.1371/journal.pone/0150333.

Niehaus A., and Ydenberg R. (2006) Ecological factors associated with the breeding and migratory phenology of high- latitude breeding western sandpipers. Polar Biol., 30, 11-17.

NRC. (2011) Climate stabilization targets: emissions, concentration, and impacts over decades to millennia. National Research Council. The National Academies Press, Washington, DC, USA.

NTPC. (2013) Energy alternatives, Northwest Territories. Northwest Territories Power Corporation, NT, Canada.

Painter T., Berisford D., Boardman J., Bormann K., Deems J., Gehrke F., Hedrick A., Joyce M., Laidlaw R., Marks D., Mattmann C., McGurk B., Ramirez P., Richardson M., Skiles M., Seidel F., and Winstral A. (2016) The Airborne Snow Observatory: Fusion of scanning lidar, imaging spectrometer, and physically-based modeling for mapping snow water equivalent and snow albedo. Remote Sensing of Environment, 184, 139-152.

Paquet E., Laval M., Basaleaev M., Belov A., Eroshenko E., Kartyshov V., Struminsky A., and Yanke V. (2008) An application of cosmic-ray neutron measurements to the determination of the snow water equivalent. Proceedings of the 30th International Cosmic Ray Conference. Mexico City, Mexico, 2008 Vol. 1 (SH) 761-764.

Peterson N., and Brown J. (1975) Accuracy of snow measurements. In Proceedings of the 43rd Annual Meeting of the Western Snow Conference, Coronado, California, 1-5.

Pomeroy J., and Gray D. (1995) Snowcover: Accumulation, relocation and management. NHRI Science Report No 7.

Pomeroy J., Gray D., Brown T., Hedstrom N., Quinton W., Granger R., and Carey S. (2007) The cold regions hydrological model: A platform for basing process representation and model structure on physical evidence. Hydrol. Processes. 21(19), 2650-2667.

Pulliainen J. (2006) Mapping of snow water equivalent and snow depth in boreal and sub-Arctic zones by assimilating space-borne microwave radiometer data and ground-based observations. Remote Sensing of Environment, 101(2), 257-269.

Qu X. and Hall A. (2006) Assessing snow albedo feedback in simulated climate change. J. Climate, 19, 2617-2630.

Rasmussen R., Baker B., Kochendorfer J., Meyers T., Landolt S., Fischer A. P., Black J., Thériault M., Kucera P., Gochis D., Smith C., Nitu R., Hall M., Ikeda K., and Gutmann E. (2012) How well are we measuring snow: the NOAA/FAA/NCAR winter precipitation test bed, Bull. Am. Meteorol. Soc., 93, 811–829.

Rees A., English M., Derksen C., Toose P., and Silis A. (2014) Observations of late winter Canadian tundra snow cover properties. Hydrol. Process. 28, 3962-3977. doi: 10.1002/hyp.9931

Rind D., Healy R., Parkinson C., and Martinson D. (1995) The role of seas ice in 2 X CO2 climate model sensitivity, I: The total influence of sea ice thickness and extent. Journal of Climate 8, 449-463.

Rosolem R., Shuttleworth W., Zreda M., Franz T., Zeng X., andKurc S. (2013) The effect of atmospheric water vapor on neutron count in the cosmic-ray soil moisture observing system. J. Hydrometeorol., 14(5), 1659-1667.

Roy A., Royer A., and Turcotte R. (2010) Improvement of springtime stream flow simulations in a boreal environment by incorporating snow-covered area derived from remote sensing data. J. Hydro., 390(1-2), 35-44.

Schattan P., Baroni G., Oswald S., Schöber J., Fey C., Kormann C., Huttenlau M., and Achleitner S. (2017) Continuous monitoring of snowpack dynamics in alpine terrain by aboveground neutron sensing. Water Resour. Res., 53, 3615-3634. doi:10.1002/2016WR020234.

Schiermeier, Q. (2006) Arctic stations need human touch. Nature, 441, 133. doi: https://doi.org/10.1038/441133a.

Schrön M., Rosolem R., Köhli M., Piussi L., Schröter I., Iwema J., Kögler S., Oswald S., Wollschläger U., Samaniego L., Dietrich P., and Zacharias S. (2017) The cosmic-ray neutron rover - mobile surveys of field soil moisture and the influence of roads. Water Resour. Res., e-Print: arXiv:1709.04756 [physics.geo-ph].

Schwab E., and Pitt M. (1991) Moose selection of canopy cover types related to operative temperature, forage, and snow depth. Can. J. Zool., 69(12), 3071-3077. doi:10.1139/z91-431.

Seebacher F., and Post E. (2015) Climate change impacts on animal migration. Climate Change Responses, 2, 5.

Seidel K., and Matinec J. (2004) Remote sensing in snow hydrology: runoff modelling effect of climate change. Praxis Publishing, Chichester, UK.

Shannon W. (1968) Snow surveying by electronic telemetry. Paper presented at 36th Western Snow Conference, pp. 568-98.

Sigouin M., and Si B. (2016) Calibration of a non-invasive cosmic-ray probe for wide area snow water equivalent measurement. The Cryosphere, 10, 1181-1190, https://doi.org/10.5194/tc-10-1181-2016.

Smith F., Cooper C., and Chapman E. (1967) Measuring snow depth by aerial photogrammetry. Paper presented at 35th Western Snow Conference, pp. 66-72.

SnowHydro. (2004) SWE core tube. Retrieved from http://www.snowhydro.com/column3.htm.

.

Statistics Solutions. (2013) Data analysis plan: Bivariate (Pearson) correlation. Retrieved from http://www.statisticssolutions.com/academic-solutions/member-resources/member-profile/data-analysis-plan-templates/data-analysis-plan-bivariate-pearson-correlation/profile/data-analysis-plan-templates/data-analysis-plan-bivariate-pearson-correlation/

Stevenson R., and Bryant M. (2000) Climate change and constraints on breeding. Nature, 406, 366-367.

Stewart R., Pomeroy J., and Lawford R. (2011) The drought research initiative: A comprehensive examination of drought over the Canadian Prairies. Atmos. Ocean. 49(4), 298-302.

Sturm M. (1999) Self-recording snow depth probe. CRREL Factsheet. Cold Regions Res. Eng. Lab., Hannover, N. H.

Sturm M., Taras B., Liston G., Derksen C., Jones T., and Lea J. (2010) equivalent using snow depth data and climate classes equivalent using snow depth data and climate classes. Hydrometeorology, 11, 1380-1394.

Takala M., Luojus K., Pulliainen J., Derksen C., Lemmtyinen J., Kärnä J., Koskinen J., and Bojkov B. (2011) Estimating northern hemisphere snow water equivalent for climate research through assimilation of space-borne radiometer data and ground-based measurements. Remote Sensing of Environment, 115(12), 3517-3529.

Thirel G., Salamon P., Burek P., and Kalas M. (2013) Assimilation of MODIS snow cover area data in a distributed hydrological model using the particle filter. Remote Sensing of the Environment, 5(11), 5825-5850.

Tollefson J. (2017) Major report prompts warnings that the Arctic is unraveling. Article. doi:10.1038/nature.2017.21911

Turcan J., and Loijens J. (1975) Accuracy of snow survey data and errors in snow sampler measurements. Proc. 32nd East. Snow. Conf., 2-11.

Turcotte R., Lacombe P., Dimnik C., and Villeneuve J. (2004) Prévision hydrologique distribuée 308-320.pour la gestion des barrages publics du Québec. Can. J. Civ. Eng., 31(2), 308-320.

Vershinina L. (1985) The use of aerial gamma surveys of snowpack for spring snowmelt runoff forecasts. Hydrological Applications of Remote Sensing and Remote Data Transmission, Proc. Hamburg Symp, August 1985, IAHS Publ. No. 145, pp. 411-420.

Waiser T., Morgan C., Brown D., and Hallmark C. (2007) Insitu characterization of soil clay content with visible near-infrared diffuse reflectance spectroscopy. Soil Science Society of America Journal, 71(2), 389. doi:10.2136/sssaj2006.0211.

White D., Hinzman L., Alessa J., Cassano M., Chambers K., Falkner J., and Francis J. (2007) The arctic freshwater system: Changes and impacts. Journal of Geophysical Research, 112, G04S54.

Williams M., Erickson T., and Petrzelka J. (2010) Visualizing meltwater propagation through snow at the centimeter-to-meter scale using a snow guillotine. Hydrol. Process., 24(15), 2098-2110.

Woo K. (1980) Hydrology of a small lake in the Canadian high arctic. Arct. Alp. Res., 12(2), 2270235. doi:10.2307/1550519.

Work R., Stockwell H., Freeman T., and Beaumont R. (1965) Accuracy of field snow surveys, western United States, including Alaska. U.S. Army Corps of Engineers, Cold Regions Research and Engineering Lab: Hanover, New Hampshire, pp 43.

Wrona E. (2016) Evaluation of novel remote sensing techniques for soil moisture monitoring in the Western Canadian Arctic. MSc Thesis. University of Guelph.

Zreda M., Desilets D., Ferré T., and Scott R. (2008) Measuring soil moisture content non-invasively at intermediate spatial scale using cosmic-ray neutrons. Geophys. Res. Lett., 35, L21402. doi:10.1029/2008GL035655.

Zreda M., Shuttleworth W., Zeng X., Zweck C., Desilets D., Franz T., and Rosolem R. (2012) COSMOS: The Cosmic-ray Soil Moisture Observing System. Hydrol. Earth Syst. Sci., 16, 4079-4099.